

VEHICLE THERMAL CONTROL
WITH A
VARIABLE AREA INLET

THESIS

Thomas R. Layne, Captain, USAF
AFIT/GAE/ENY/95D-15

19960118 040

DEPARTMENT OF THE AIR FORCE
AIR UNIVERSITY
AIR FORCE INSTITUTE OF TECHNOLOGY

DTIC QUALITY INSPECTED 3

Wright-Patterson Air Force Base, Ohio

DISTRIBUTION STATEMENT A

Approved for public release;
Distribution Unlimited

AFIT/GAE/ENY/95D-15

Accession For	
NTIS CRA&I	<input checked="checked" type="checkbox"/>
DTIC TAB	<input type="checkbox"/>
Unannounced	<input type="checkbox"/>
Justification	
By	
Distribution /	
Availability Codes	
Dist	Avail and/or Special
A-1	

**VEHICLE THERMAL CONTROL
WITH A
VARIABLE AREA INLET**

THESIS

**Thomas R. Layne, Captain, USAF
AFIT/GAE/ENY/95D-15**



DTIC QUALITY INSPECTED 3

DISTRIBUTION STATEMENT A
Approved for public release;
Distribution Unlimited

AFIT/GAE/ENY/95D-15

VEHICLE THERMAL CONTROL WITH A VARIABLE AREA INLET

THESIS

Presented to the Faculty of the School of Engineering
of the Air Force Institute of Technology Air University

In Partial Fulfillment of the
Requirements of the Degree of
Master of Science in Aeronautical Engineering

Thomas R. Layne

Captain, USAF

December 1995

Approved for public release; distribution unlimited

ACKNOWLEDGMENTS

A successful senior officer whom I highly respected had said, "much of my success comes from the fact that I have always been surrounded by great people". With the completion of this thesis, I now truly understand the meaning of his statement. The people that surrounded me during this research were second to none.

First of all, I would like to thank the technicians Jay Anderson, Marc Deriso, Jan LaValley, Charlie Mcneely, Andy Pitts, and Dan Rioux. They all took a personal interest in the success of this thesis.

Secondly, I would like to thank my committee members Dr Beran, Lt Col Bowman, and Dr Ridgely. They all made time for my questions and they treated me like I was their own thesis student.

Thirdly, I would like to thank my advisor Dr Franke. His enthusiasm provided me with motivation and his foresight kept me prepared throughout the entire thesis process. I really appreciated the freedom that he gave me and I admired his ability to put the research on track when it started to stray.

Most importantly, I would like to thank my wife Rachael. Over the past months her sacrifices have far surpassed mine and never once did she complain. Even during the times that were very difficult for her, she still managed to smile. I am very lucky to have a wife that is as patient, encouraging, and loving as she.

Thomas R. Layne

TABLE OF CONTENTS

ACKNOWLEDGMENTS	ii
LIST OF FIGURES	v
LIST OF TABLES	viii
LIST OF SYMBOLS	ix
ABSTRACT.....	xii
I. INTRODUCTION.....	1
Outline.....	7
II. FUNDAMENTAL PRINCIPLES	8
Feedback Control	8
Heat Transfer	11
Thermal Control Example Using a Simple Model	17
Thermal Control, Actual Model.....	21
III. EXPERIMENTAL & ANALYTICAL SET UP.....	24
Hardware Model Description.....	24
Instrumentation	26
Data Acquisition System.....	27
Simulation Model	28
IV. RESULTS	33
Component Test Results	33

Hardware & Simulation Model Correlation	39
Proportional Controller Design.....	45
Linearized Plant & Root Locus Controller Design.....	53
Matlab Nonlinear Toolbox Controller Design.....	60
Noise, Changing Reference Temperature, and Experimental PID Data	64
V. APPLICATION	68
Controller Design Approach	68
VI. CONCLUSIONS	71
VII. RECOMMENDATIONS	73
REFERENCES	74
APPENDIX A. Air Properties Analysis	75
APPENDIX B. Conduction Analysis	77
APPENDIX C. Lab View™ Subroutine.....	80
APPENDIX D. Inlet Dynamics Test	84
APPENDIX E. Component Orientation Test.....	86
APPENDIX F. Convection Coefficient Test	89
VITA	94

LIST OF FIGURES

Figure 1.	Uncontrolled vs. Controlled Component Surface Temperature.....	5
Figure 2.	Illustration of an Open-Loop Control Model.....	8
Figure 3.	Illustration of a Closed-Loop Control Model	9
Figure 4.	Illustration of One-Dimensional Heat Transfer by Conduction	12
Figure 5.	Illustration of Simplified Model & Control Volume.....	17
Figure 6.	Simplified Model Temperature Response to a Step Heat Input.....	18
Figure 7.	Simplified Model Temperature Response to a Ramp Heat Input.....	19
Figure 8.	Simplified Model Temperature Response to a Sinusoid Heat Input	20
Figure 9.	Illustration of Actual Model & Control Volume	21
Figure 10.	Illustration of Physical Model.....	24
Figure 11.	Component Schematic	25
Figure 12.	Illustration of Closed-Loop Control Model	29
Figure 13.	Illustration of the SIMULINK™ Actuator Plant.....	30
Figure 14.	Illustration of Duct Inlet Curve.....	31
Figure 15.	Illustration of the SIMULINK™ Inlet Plant.....	31
Figure 16.	Illustration of the SIMULINK™ Thermal Plant	32
Figure 17.	Family of Curves for the Inlet Model	35
Figure 18.	Illustration of Component Orientation	36
Figure 19.	Surface Temperature vs. Component Orientation Test Data	37

Figure 20.	Dimensionless Representation of Heat Transfer Coefficient.....	38
Figure 21.	Inlet Leakage Correlation	40
Figure 22.	13 % Leakage Verification Plot.....	41
Figure 23.	Actual Heat Generation Rate to Thermal Capacity Ratio.....	42
Figure 24.	Comparison of Simulation and Hardware Model Responses Condition 1, Gain-0.5, Ref Temp-35(C), Freestream Airspeed-8.9(m/s).....	47
Figure 25.	Comparison of Simulation and Hardware Model Responses Condition 1, Gain-8, Ref Temp-35(C), Freestream Airspeed-8.9(m/s).....	47
Figure 26.	Comparison of Simulation and Hardware Model Responses Condition 3, Gain-8, Ref Temp-50(C), Freestream Airspeed-8.9(m/s).....	48
Figure 27.	Comparison of Simulation and Hardware Model Responses Condition 8, Gain-8, Ref Temp-35(C), Freestream Airspeed-26.8(m/s).....	48
Figure 28.	Gain Values for the Scheduled Proportional Controller	51
Figure 29.	Condition 1, Scheduled Gain-20.14, Ref Temp-35(C), Freestream Airspeed-8.9(m/s).....	51
Figure 30.	Condition 3, Scheduled Gain-4.72, Ref Temp-50(C), Freestream Airspeed-8.9(m/s).....	52
Figure 31.	Condition 8, Scheduled Gain-6.72, Ref Temp-35(C), Freestream Airspeed-26.8(m/s).....	52
Figure 32.	Root Locus Diagram with a zero at $s=-0.1$	57
Figure 33.	Comparison of Scheduled Gain (P) and PD Controllers Condition 1, Ref Temp-35(C), Freestream Airspeed-8.9(m/s).....	58
Figure 34.	Comparison of Scheduled Gain (P) and PD Controllers Condition 3, Ref Temp-50(C), Freestream Airspeed-8.9(m/s).....	59
Figure 35.	Comparison of Scheduled Gain (P) and PD Controllers Condition 8, Ref Temp-35(C), Freestream Airspeed-26.8(m/s).....	59
Figure 36.	NCD Design Window with PID Controller Response.....	61

Figure 37.	Root Locus Diagram of NCD PID Controller	62
Figure 38.	Comparison of PD and PID Controllers Condition 1, Ref Temp-35(C), Freestream Airspeed-8.9(m/s).....	63
Figure 39.	Comparison of PD and PID Controllers Condition 3, Ref Temp-50(C), Freestream Airspeed-8.9(m/s).....	63
Figure 40.	Comparison of PD and PID Controllers Condition 8, Ref Temp-35(C), Freestream Airspeed-26.8(m/s).....	64
Figure 41.	Actual Sample of White Noise Added to Thermocouple Signal	65
Figure 42.	PD & PID Controllers with Noise and Modified Control Schedule Freestream Airspeed- 8.9(m/s).....	65
Figure 43.	Comparison of Simulation and Hardware Responses to Similar PID(lab) Controllers. Freestream Airspeed- 26.8(m/s).....	67

LIST OF TABLES

Table 1. Experimental Study of Drag Sources on XP-41	3
Table 2. Estimated Conductive Heat Losses for Different Operating Conditions	22
Table 3. Estimated Radiative Heat Losses for Different Operating Conditions	23
Table 4. Measurement Uncertainty	34
Table 5. Test Condition Values.....	45
Table 6. Scheduled Proportional Controller Data	50

LIST OF SYMBOLS

A	Area (m^2)
Bi	Biot Number, hL / k
c	Constant, $c = cPr^n$
c	Constant
C	Thermal Capacitance, $\rho c_p V$ (J / K)
c_p	Specific Heat ($\text{J} / \text{kg K}$)
CV	Control Volume (m^3)
E	Energy (J)
$G(s)$	s-Domain Plant
h	Convection Heat Transfer Coefficient ($\text{W} / \text{m}^2 \text{K}$)
G	Controller Gain
k	Thermal Conductivity (W / mK)
k_f	Fluid Thermal Conductivity (W / mK)
K_d	Controller Derivative Gain
K_i	Controller Integral Gain
K_p	Controller Proportional Gain
$K(s)$	State Space Controller
l	Length (m)
L	Characteristic Length (m)
m	Exponent in Empirical form of Nusselt Number

n	Exponent in Empirical form of Nusselt Number
Nu	Nusselt Number, hL / k_f
p	Timestep
P	Controller Output (pulses / sec)
Pr	Prandtl Number, ν / α
q_{cond}	Rate of Heat Conducted (W)
$q_{cond,x}$	Rate of Heat Conduction in X-Direction (W)
q_{conv}	Rate of Heat Convected (W)
q_{gen}	Thermal Energy Generation (W)
q_{rad}	Rate of Heat Radiated (W)
q_{stor}	Rate of Heat Stored (W)
q_x	Heat Transfer Rate in X-Direction (W)
q'	Unit Power Input (W)
Q	Heat energy (J)
R_{cd}	Conduction Resistance (K/W)
R_{cv}	Convection Resistance (K/W)
Re	Reynolds Number, VL / ν
s	Laplace Transform Variable
t	Time (sec)
T^*	Dimensionless Temperature $((T(y)-T_l) / (T_\infty - T_l))$
T_1	Controlled Temperature (C)
T_{10}	Nominal Controlled Temperature (C)

T_{diff}	$(T_{ref} - T_{\infty})$ Reference minus Ambient Temperature Difference (C)
T_{film}	Average Temperature between Freestream Ambient and Surface Temperature (C)
T_{ref}	Reference Temperature (C)
T_{surr}	Surroundings Temperature (C)
T_{∞}	Ambient Temperature (C)
$U(s)$	s-Domain Input
V	Velocity (m/s)
V	Volume (m^3)
V_o	Nominal Test Section Airspeed (m/s)
ΔV	Change in Test Section Airspeed (m/s)
V_{∞}	Freestream Airspeed (m/s)
W_o	Work (J)
x	Direction of heat conduction (m)
y	Direction normal to surface (m)
y^*	Dimensionless y (y/L)
$Y(s)$	s-Domain Output
α	Thermal Diffusivity, $k / \rho c_p$ (m^2 / s)
ε	Emissivity
ν	Kinematic Viscosity (m^2 / s)
ρ	Density (kg / m^3)
σ	Stefan Boltzmann Constant ($5.67 \times 10^{-8} \text{ W} / m^2 K^4$)
ω	Frequency ($1 / s$)

ABSTRACT

This study developed a variable area inlet and controller that regulated the temperature of an electrical component with ram air. The intent of the variable area inlet was to reduce vehicle drag by eliminating inefficiencies associated with component cooling and fixed area inlets. These inefficiencies arise from vehicles moving at varying speeds through varying air temperatures. The hardware model consisted of an electrical component mounted inside a right-circular cylindrical duct. The variable area inlet, mounted in the front of the duct, consisted of a butterfly valve that was actuated by a stepper motor. The stepper motor was controlled by a software subroutine that was run on a personal computer. The controller acted on the feedback signal of a thermocouple that was mounted on the electrical component. The system was successful in regulating the component temperature. A nonlinear simulation model was built and the thermal plant in the simulation was based on the electrical component's empirically derived Nusselt number. Proportional, Proportional-Derivative (PD), and Proportional-Integral-Derivative (PID) controllers were built and tested. The PD and PID controllers did not appear to need any gain scheduling for the varying speed and temperature conditions. Lastly, a general design process was detailed.

I. INTRODUCTION

Aircraft, automobiles, and many other types of vehicles use ambient air as a heat sink for cooling components. Many rely heavily on ram air for forced convection cooling with fans to augment the ram air at low speeds. The use of ram air for forced convection cooling has many advantages. The most significant advantage is that it is available as long as the vehicle is moving. In addition, ram air ducts are lightweight, reliable, and require low maintenance.

Many vehicles use fixed area inlets to bring ram air into compartments or around components. A characteristic of the fixed inlet design is that the speed of the ducted air generally increases with vehicle speed. The speed of the ducted air used for cooling is important to the designer because higher speeds improve the rate of convection heat transfer. In addition, the temperature of the ducted air is also important. Lower ducted air temperatures improve the rate of convection heat transfer.

The combination of vehicle speed, ambient air temperature, and inlet characteristics pose trade-offs to the designer of fixed inlets. One design approach is to design the inlets for low speeds to reduce the need for augmented fan cooling. These designs often have large inlets and, unfortunately, they tend to provide excess air at high speeds. Another approach is to design the inlets for high speeds to reduce the vehicle-air interaction, possibly reducing drag. These designs usually have smaller inlets and thus they require more augmented fan cooling at low speeds.

As mentioned earlier, a further complication to the designer is the need to consider the range of ambient air temperatures that will be used for cooling. Ambient air temperatures vary with elevation, region, and time. For example, northern winter air temperatures are often below freezing (0 deg C) and southern summer air temperatures are often above 38 deg C. It becomes obvious that fixed inlet designs cannot be optimal for all operating conditions. Furthermore, fixed inlets may often be oversized to accommodate severe environmental conditions. Specifically, oversized inlets may increase drag losses, thus reducing vehicle performance and efficiency.

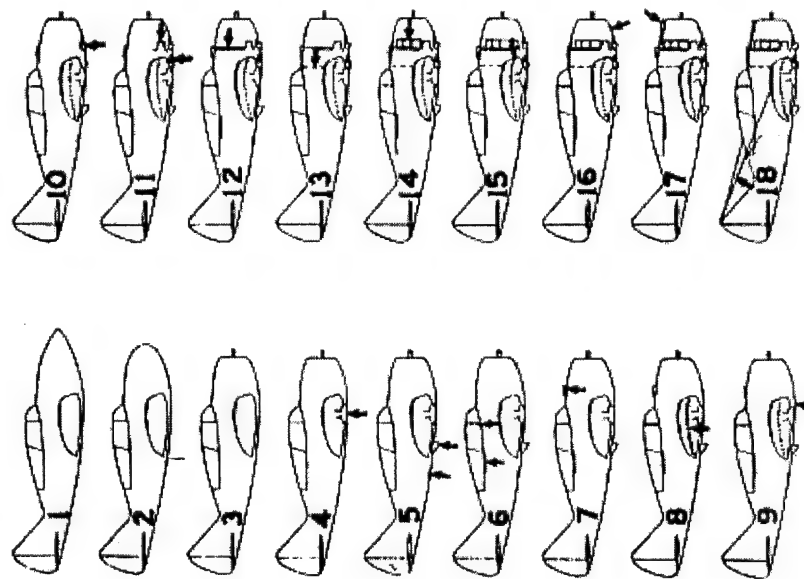
An investigation was performed to locate research that had quantified the drag losses associated with internal cooling airflow. In an experimental study of drag sources on the Seversky XP-41 aircraft, a 25.2 percent increase to the drag coefficient was recognized by modifications that were associated with internal cooling airflow [1]. These modifications are shown in Table 1 and include: the addition of an oil cooler - Line 5, the opening of the cowling exit - Line 12, the opening of the accessory exit - Line 13, and the removal of the cowling fairing and seals - Line 14. In addition, Carr [2] indicated that a part of the aerodynamic drag of an automobile results from 'cooling system drag'. Carr defined automobile 'cooling system drag' as the drag difference when cooling air intakes were open and when cooling air intakes were closed. In his study he reported on the 'cooling system drag' from 100 different automobiles that were tested in the MIRA Full-Scale Wind Tunnel between 1990 and 1994. He found that the drag coefficient ranged between 0.006 and 0.041 with a mean value of 0.019, which was approximately 6% of the typical total drag coefficient.

Table 1. Experimental Study of Drag Sources on XP-41 [1]

Condition number	Description	C_D ($C_L = 0.15$)	ΔC_D	ΔC_D , percent ^a
1	Completely faired condition, long nose fairing	0.0166		
2	Completely faired condition, blunt nose fairing	.0169		
3	Original cowl added, no airflow through cowl	.0166	0.0020	12.0
4	Landing-gear seals and fairing removed	.0188	.0002	1.2
5	Oil cooler installed	.0205	.0017	10.2
6	Canopy fairing removed	.0203	-.0002	-1.2
7	Carburetor air scoop added	.0209	.0006	3.6
8	Sanded walkway added	.0216	.0007	4.2
9	Ejector chute added	.0219	.0003	1.8
10	Exhaust stacks added	.0225	.0006	3.6
11	Intercooler added	.0236	.0011	6.6
12	Cowling exit opened	.0247	.0011	6.6
13	Accessory exit opened	.0252	.0005	3.0
14	Cowling fairing and seals removed	.0261	.0009	5.4
15	Cockpit ventilator opened	.0262	.0001	.6
16	Cowling venturi installed	.0264	.0002	1.2
17	Blast tubes added	.0267	.0003	1.8
18	Antenna installed	.0275	.0008	4.8
Total			0.0109	

^a Percentages based on completely faired condition with long nose fairing.

Airplane Condition

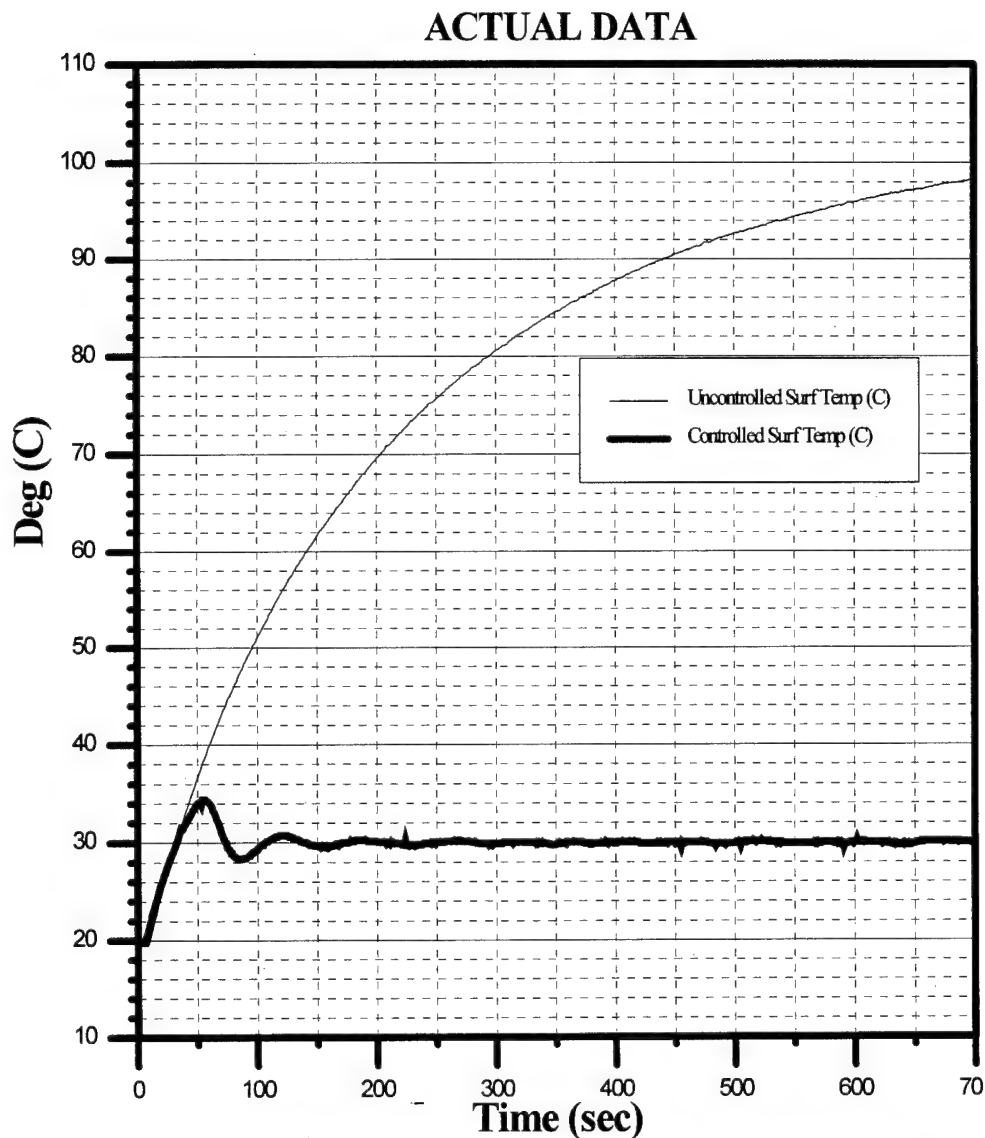


With the inefficiencies associated with the fixed area inlet and the percentage estimates of the drag coefficient resulting from internal cooling, there appeared to be an opportunity to improve vehicle efficiency and performance. This opportunity was the motivation that led to the development of the variable area inlet.

During the conceptual stage of the development it was determined that by building a working model of an inlet, the concept could be proven and a general design process could be documented to aid in future implementations. Consequently, this thesis had two primary objectives. The first objective was to develop a working hardware model to validate the concept of regulating a component's temperature with ram air and a variable area inlet. The second objective was to create a general design process. To describe the first objective more thoroughly, the prototype inlet was designed to automatically minimize the inlet area throughout the range of all vehicle speeds and all ambient temperatures while providing sufficient air for forced convection cooling. In other words, this inlet was designed to regulate ram air over a component to control the temperature of that component to a desired temperature. To illustrate, a component will be generating energy. If left alone with no convection cooling, its steady state temperature will stabilize outside allowable tolerances. However, by use of a variable area inlet, ram air, and feedback control, the components temperature will be regulated to a desired value while minimizing the airflow over the component (see Figure 1).

Temperature control is not a new subject. Thermostats have been used in houses for decades and fans have been used to control temperatures for centuries. This design differs from many conventional temperature control applications because it is not an

on/off control design. The inlet position is variable, allowing it to find the optimal position in the changing velocity and temperature environment. In addition, this research takes a unique approach to modeling the thermal system by using air velocity to adjust the convection coefficient (Nusselt number).



* Controlled component temperature regulated to 30 deg C, uncontrolled component temperature includes free convection but not forced convection cooling

Figure 1. Uncontrolled vs. Controlled Component Surface Temperature

To design a controller for this system, a thermal control model was needed. Based on a background search of thermal control models, it appeared that most control models were derived from an energy balance (Conservation of Energy). In addition, the same background search revealed that almost all control models such as those in Franklin et al. [3], Close & Fredrick [4], and Cannon [5] treat the convection coefficient as a constant. Franklin et al. provide an example of a heat exchanger that adjusts fluid A's inlet valve position in order to control fluid B's outlet temperature. Although the temperature control concept is similar to the one in this thesis, the approach is different. In their example, Franklin et al. did not deal with a changing convection coefficient. They treated the convection heat transfer coefficient between the two fluids as a constant, much like a conduction term.

The thermal control model for this thesis requires the convection coefficient to be variable because the input to the thermal control model is cooling airspeed. The purpose of the variable area inlet is to vary the cooling airspeed, resulting in a changing convection coefficient, to keep the component at a desired temperature. One possible reason for the lack of temperature control work based on a varying convection coefficient is that a nonconstant convection coefficient complicates the mathematics of the energy equation. A varying convection term makes the input variable, velocity, nonlinear by raising it to a power less than one. In addition, it causes the output variable, surface temperature, to be multiplied by the input variable. In short, no thermal control models could be found for a varying convection coefficient where cooling airspeed was the input variable.

Outline

This thesis consists of seven chapters including this introduction. Chapter II will present fundamentals of control theory and heat transfer that were used in this study. These fundamentals form the foundation for the control logic and they define the thermal system in terms of the input variable (velocity) and the output variable (temperature). These fundamentals are then connected in a simple example to provide additional insight into thermal control and Laplace transformations. Then, the control model used in the simple example was modified to obtain the specific thermal control model that was used in the simulation model. Chapter III discusses the set-up and operation of the hardware and simulation models. The hardware model was specifically required to meet the first objective of this thesis. The simulation model was used for controller design. Chapter IV contains all the results. The first part of Chapter IV contains the results of component tests. These tests were conducted to understand the hardware characteristics that needed to be modeled in the simulation. The chapter then discusses the steps that were taken to improve the responses between the hardware and simulation models. The remainder of Chapter IV evaluates the results of different controllers. The first controller design starts out simple by being a fixed proportional gain. The second controller design improves the temperature control performance by scheduling the proportional gain as a function of freestream airspeed and temperature difference. The third controller design uses root locus techniques and a linearized thermal plant. The last controller design requires the use of MATLAB's Nonlinear Control Design Toolbox. Chapter V details a general design process. Chapters VI and VII provide conclusions and recommendations, respectively.

II. FUNDAMENTAL PRINCIPLES

Control Theory

Control theory is the discipline of modeling, analyzing, and controlling input-output plant system processes with emphasis on their time and frequency response. Control theory is not based on physical laws like heat transfer. It is a mathematical process of causing a system output variable to react in a desired way to a specified input. This research will be evaluating a system that will be using the control variable, velocity (V), to regulate the output variable, surface temperature (T_I), to a specified reference temperature (T_{ref}).

Control systems are often represented by block diagrams, and a generic open-loop model is illustrated in Figure 2. The plant is a model of the system to be controlled and is defined by a set of differential equations.

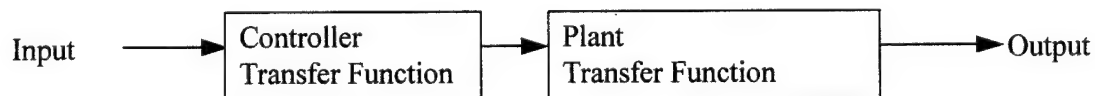


Figure 2. Illustration of an Open-Loop Control Model

The above diagram also includes the label called 'transfer function'. A transfer function is the plant, controller, and/or system's differential equations arranged in an input-output format. For example, given any input, the transfer function will model the control system/plant and provide the modeled system's output.

As stated earlier, a plant is modeled by a set of differential equations. In this research, the plant is a thermal system that will be represented by a differential equation based on an energy balance. If the system is linear, the differential equations can be converted to the s-domain using Laplace transformations. After the s-domain transfer function $G(s)$ is obtained, s-domain input functions $U(s)$ are simply multiplied by it to produce the output response $Y(s)$, where $Y(s)=G(s)U(s)$. The system's time response to the input function can be obtained by taking the inverse Laplace transform. This research will use a closed-loop control system model that is illustrated in block diagram form in Figure 3.

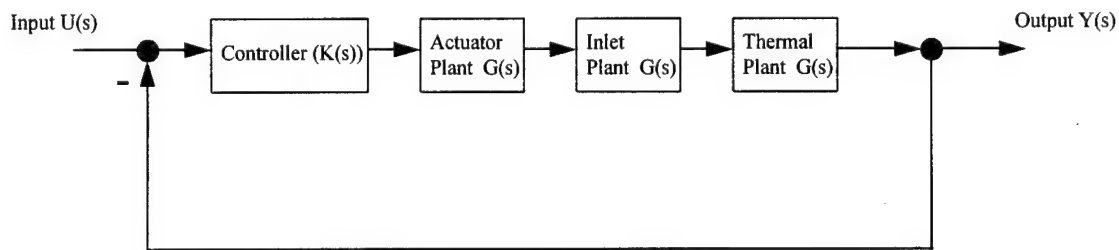


Figure 3. Illustration of a Closed-Loop Control Model

The closed-loop feedback system modeled in Figure 3 can be more specifically labeled as a negative unity feedback control system. The main objective of negative unity feedback control is to drive the difference between the input reference value and the output variable value to zero with increasing time, resulting in a well performing, stable system. There are many ways to define stable or stability. Physically, it means that if a bounded input is applied to the plant and/or system, the respective response will decay

with time (remain bounded). An unstable system response will diverge from the reference value with time. Defined in the s-domain, the roots of the denominator in the closed-loop s-domain transfer function must have negative real parts for stability. The controller can do many things. In some applications, it can make an unstable plant stable. In other applications, it can improve the plant's performance to an input or reference value. The controller in this thesis will be designed for temperature regulating performance. Furthermore, there are a number of ways to analyze a control system. If the system is modeled in s-domain transfer function form, the differential equations must be linear and time-invariant. If they pass this test, there are a number of tools that can be used to analyze the system and design a controller. The root locus diagram is a specific tool used in this research.

It was stated earlier that control theory is particularly interested in the input-output time response of a system. Because of this interest, there exists a standard set of time based inputs. When these standard inputs are applied to the system of interest, time-based performance and stability measures can be made to quantify the system's response. The step input will be used in this research.

Lastly, there is another way to represent the differential equations arranged in transfer function form. It is called state space representation. State space reduces all the higher order differential equations to a set of first order differential equations. State space will be used to model the thermal plant in the simulation model (concepts from this section taken from Franklin et al. [3]).

Heat Transfer

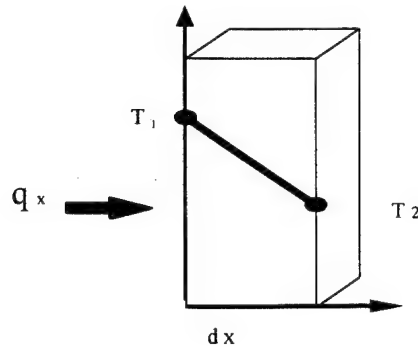
To generate a representative control model of the system being analyzed, an energy balance was performed on a control volume. When performing an energy balance on a control volume at an instant in time, thermal energy can be accounted for by either being transferred through a surface, transformed (generated) throughout the volume, or stored within the volume.

Thermal energy can flow or be transferred through a surface of the control volume, from a region of high temperature to a region of low temperature, by any of three modes called conduction, convection, or radiation. This heat transfer and these three modes are all described by different rate equations. Although all three modes of heat transfer are present in this thesis, convective heat losses are much greater than both conductive and radiative heat losses.

To start out, the conduction mode is recognized by the absence of any bulk motion in the medium that the heat is flowing through. The conduction rate equation is known as Fourier's law, illustrated in Figure 4, and written as

$$q_{\text{cond},x} = -kA \frac{dT}{dx} \quad (1)$$

This states that the heat transfer rate in the x-direction equals the thermal conductivity k of the material multiplied by the surface area A normal to the temperature gradient, and multiplied by the temperature gradient in the x-direction. The conductivity term k is a material property that characterizes the ability of the material to transfer thermal energy.



*Area (A) is represented by the side of the cube that is normal to q_x

Figure 4. Illustration of One-Dimensional Heat Transfer by Conduction

The second mode, called convection, includes bulk motion in the medium between the two temperature regions. Convection can be subdivided into free convection and forced convection. The bulk motion in free convection is caused by gravity and buoyancy forces that arise in the fluid by temperature variations from the heat flux. The bulk motion in forced convection is caused by some external means (fan, ram air, wind, etc.). In either case, the convection heat transfer rate equation is characterized by Newton's law of cooling

$$q_{\text{conv}} = hA(T_1 - T_{\infty}) \quad (2)$$

This states that the convection heat transfer rate equals the convection coefficient h multiplied by the surface area A and a temperature difference between the surface temperature T_1 and the freestream temperature T_{∞} . The heat transfer coefficient h is not a material property like conduction. It is based on surface properties between the two mediums. It varies with geometry, bulk motion velocity, fluid properties, and surface conditions. One of the critical tests performed in this thesis was

to empirically determine the value of the convection coefficient as a function of freestream airspeed.

The last mode of heat transfer is radiation. Radiation occurs by means of an electromagnetic wave. This mode does not need a medium to pass through. In fact, radiation attenuates the least when it is in a vacuum. For low temperature, forced convection applications, radiation heat transfer may be insignificant. Since, the radiation heat transfer rate varies as T^4 , at elevated temperatures it can be the most significant contributor to heat transfer. The radiation heat transfer rate equation is given by

$$q_{\text{rad}} = \sigma A \varepsilon (T_1^4 - T_{\text{surr}}^4) \quad (3)$$

This states that the radiation heat transfer rate equals the Stefan Boltzmann constant σ multiplied by the surface area A , surface emissivity ε , and the difference between the surface temperature T_1 raised to the fourth power and the surrounding temperature T_{surr} raised to the fourth power.

The modes of how thermal energy can be transferred have been presented, but there is a need to look at how thermal energy can be transformed. In the context of heat transfer, the transformation of energy usually implies that energy in one form is being converted to thermal energy. In this thesis, electrical energy will be converted to heat through electrical resistance (q_{gen}).

Lastly, thermal storage is the final element that appears in the energy balance used in this research. Materials, as well as systems, possess the ability to store energy. This ability is usually referred to as thermal capacity. To raise the temperature of a material, thermal energy needs to be transferred to the material and stored within it. It should be noted that if a material is undergoing a phase change, its temperature may stay relatively

constant while its internal energy changes significantly. This research will not be affected by a phase change. The rate of thermal storage is defined by

$$q_{\text{stor}} = \rho c_p V \frac{dT_1}{dt} \quad (4)$$

This states that the rate of thermal storage equals the material density ρ multiplied by the material specific heat c_p , its volume V , and its time rate of temperature change. The quantity $(\rho c_p V)$ is called thermal capacitance and it defines the amount of energy required to raise the material one degree Celsius. It will be represented as C and will appear later in this study.

For this research, the control volume consisted of a copper plate and a heating element. The top and sides of the control volume were exposed to the freestream air and the bottom of the control volume was in contact with cork. The cork was thick (approximately 1.3 cm) to reduce conductive losses through the bottom surface. By defining energy into the control volume as positive, assuming the control volume is isothermal with a temperature greater than the ambient temperature, the surrounding temperature equals the ambient temperature, and assuming the surrounding surface area is much greater than the radiating control volume surface area, the energy equation that represents the system in this thesis is

$$-\frac{kA}{x}(T_1 - T_\infty) - \sigma A \epsilon (T_1^4 - T_\infty^4) - hA(T_1 - T_\infty) + q_{\text{gen}} = \rho c_p V \frac{dT_1}{dt} \quad (5)$$

At first glance, the convection term appears simple and straightforward. Unfortunately, after closer examination of the convection coefficient h , the simplicity starts to disappear. As mentioned earlier, the convection coefficient is a very sensitive

term. It is derived by setting Fourier's law equal to Newton's law of cooling at the surface. For this case, the temperature gradient is taken in the direction that is normal to the material-air interface (y-direction represents the surface normal direction). By making the no-slip assumption at the surface energy transfer occurs by conduction. Thus,

$$h(T_1 - T_\infty) = -k_f \left. \frac{dT}{dy} \right|_{y=0} \quad (6)$$

By rearranging, we have

$$h = \frac{-k_f \left(\frac{dT}{dy} \right) \big|_{y=0}}{T_1 - T_\infty} \quad (7)$$

By redefining in dimensionless variables, we obtain

$$h = \frac{k_f}{L} \left. \frac{dT^*}{dy^*} \right|_{y^*=0} \quad (8)$$

Defining the Nusselt number as the dimensionless temperature gradient at the surface, we

see that [6]

$$Nu_L = \frac{hL}{k_f} = \left. \frac{dT^*}{dy^*} \right|_{y^*=0} \quad (9)$$

From past experimental work, the accepted empirical correlation takes the form [6]

$$Nu_L = c Re_L^m Pr^n \quad \text{where} \quad (10)$$

$$Re_L = \frac{VL}{\nu} \quad \text{and} \quad Pr = \frac{\nu}{\alpha}$$

Since the properties of air for the range of temperatures used in this thesis have little variation (see Appendix A), the Prandtl number Pr was assumed constant and is accounted for in the constant c ($c = cPr^n$). The Reynolds number Re is the ratio of inertia to viscous forces and represents the type of flow and the velocity boundary layer

thickness. The remaining constants, c and m , represent the nature of the surface geometry and the type of flow. The Nusselt number and convection coefficient for this thesis will be represented by

$$Nu_L = c Re_L^m = \frac{hL}{k_f} \quad (11)$$

The final form of the energy equation is given by

$$-\frac{kA}{x}(T_1 - T_\infty) - \sigma A \varepsilon (T_1^4 - T_\infty^4) - c \left(\frac{VL}{v} \right)_L^m \frac{k_f}{L} A (T_1 - T_\infty) + q_{\text{gen}} = \rho c_p V \frac{dT_1}{dt} \quad (12)$$

Concepts from this section were taken from [6] and [7].

Thermal Control Example Using a Simple Model

The fundamentals discussed thus far can be connected to develop a simple intuitive model that will be helpful in understanding thermal system responses and Laplace transformations for systems in equilibrium. The simple model will start from a control volume (CV) consisting of a cube of material that is in thermal equilibrium and perfectly insulated on all sides. Heat will be generated uniformly throughout the volume (turn on a heating element), and it will be assumed that the cube is isothermal (constant temperature). The control volume, shown in Figure 5, will include everything from the center of the cube to the outside of the insulation.

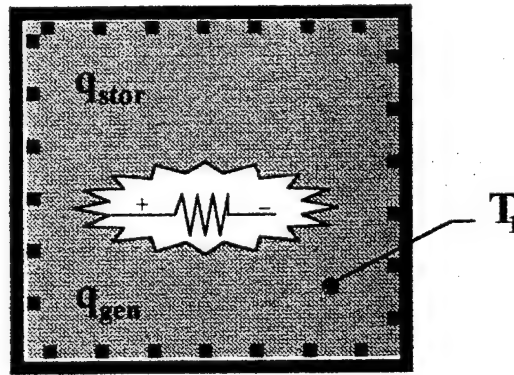


Figure 5. Illustration of Simplified Model & Control Volume

Performing an energy balance and applying the rate equations yields

$$q_{\text{gen}} = \rho c_p V \frac{dT_1}{dt} \quad (13)$$

Converting to the s-domain and letting C = thermal capacitance [8]

$$T_1(s) = \frac{q_{\text{gen}}(s)}{C s} \quad (14)$$

Therefore, the transfer function for Figure 5 is

$$\frac{T_1(s)}{q_{\text{gen}}(s)} = \frac{1}{C s} \quad (15)$$

Now, the temperature response will be evaluated against different heat generation inputs. First, a step input will be applied. Physically speaking, a step input would be similar to turning on a heating element and letting it dissipate a constant q' watts.

$$T_1(s) = \frac{1}{Cs} \left(\frac{q'}{s} \right) = \frac{q'}{Cs^2} \quad (16)$$

The time response is found by taking the inverse Laplace transform

$$T_1(t) = \mathcal{L}^{-1}(T_1(s)) = \frac{q'}{C}t \quad (17)$$

Note that the temperature response (from equilibrium) to a constant heat input is a ramp with slope q'/C . A plot of input and output is shown in Figure 6 for $q' = C = 1$.

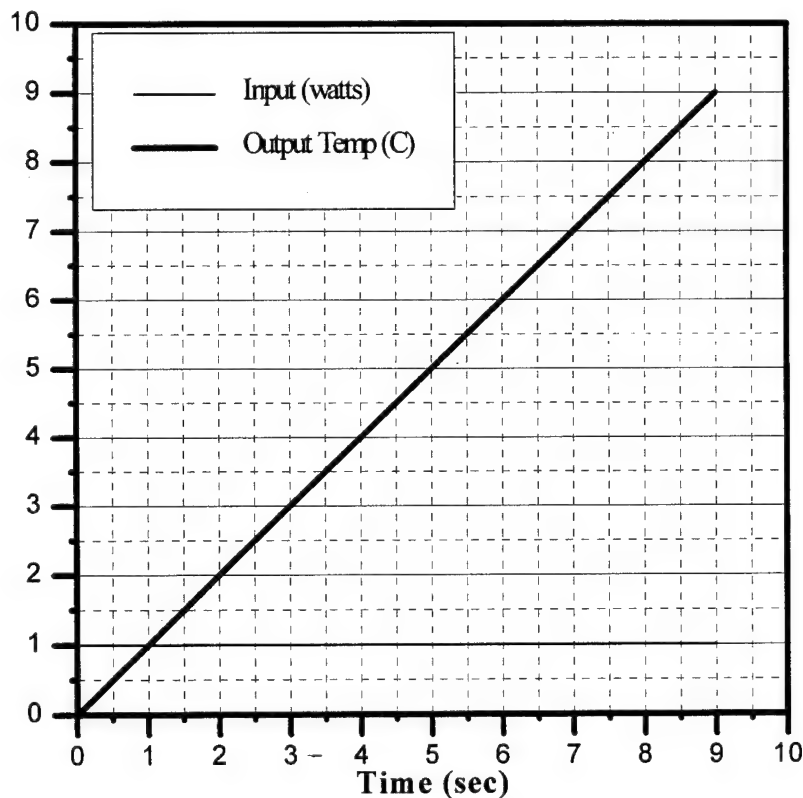


Figure 6. Simplified Model Temperature Response to a Step Heat Input

If the input is changed from a step to a ramp, the temperature responds differently.

A ramp input would be a linearly increasing input. We now have

$$T_1(s) = \frac{1}{Cs} \left(\frac{q'}{s^2} \right) = \frac{q'}{Cs^3} \quad (18)$$

The time response is found by taking the Inverse Laplace transform

$$T_1(t) = \mathcal{L}^{-1}(T_1(s)) = \frac{q'}{2C} t^2 \quad (19)$$

The input and output temperature (from equilibrium) are shown in Figure 7 for $q' = C = 1$.

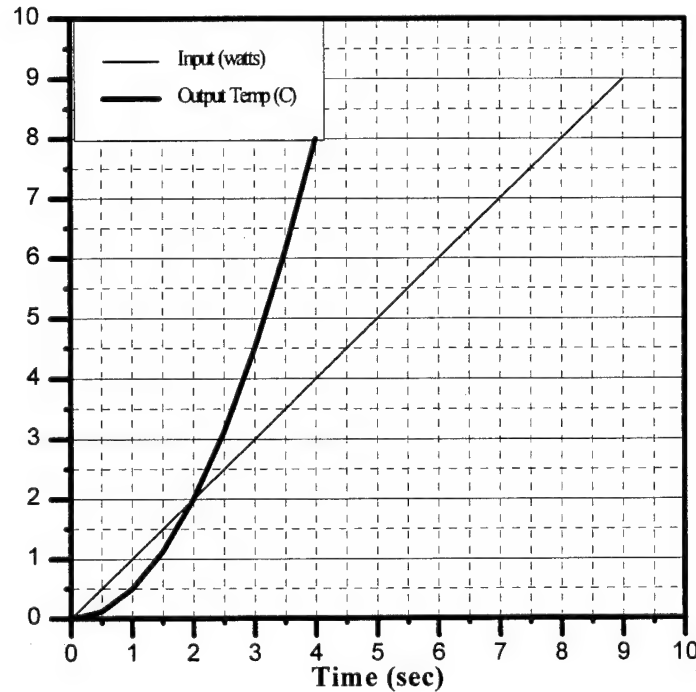


Figure 7. Simplified Model Temperature Response to a Ramp Heat Input

Lastly, the input will be changed to a sinusoid with amplitude q' and frequency ω .

For this input, a positive constant shift of q' is added so that the magnitude of q_{gen} is always non negative and heat is always being generated by the heating element. (If q_{gen}

were negative, it would mean that the heating element is a refrigeration coil!)

The time domain input is given by

$$q_{\text{gen}}(t) = q'(1 + \sin(\omega t)) \quad (20)$$

The Laplace transform of this is

$$q_{\text{gen}}(s) = q' \frac{s^2 + s\omega + s^2}{s(s^2 + \omega^2)} \quad (21)$$

Multiplying the transfer function by the input we get

$$T_1(s) = \frac{1}{Cs} \left(q' \frac{s^2 + s\omega + s^2}{s(s^2 + \omega^2)} \right) \quad (22)$$

The time response is found by taking the inverse Laplace transform

$$T_1(t) = \mathcal{L}^{-1}(T_1(s)) = \frac{q'}{C}t + \frac{q'}{C\omega}(1 - \cos \omega t) \quad (23)$$

The input and output temperature (from equilibrium) are shown in Figure 8 for $q' = C = 1$ and $\omega = 2$.

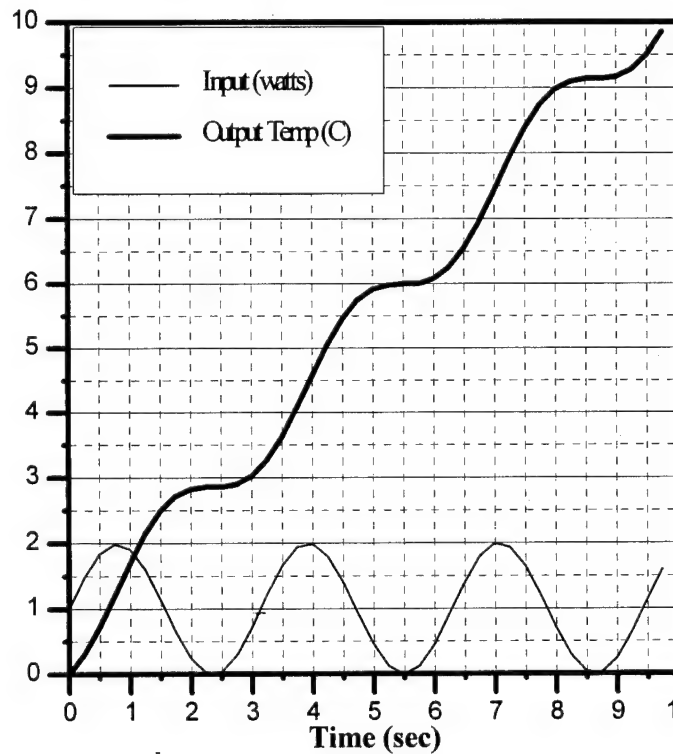
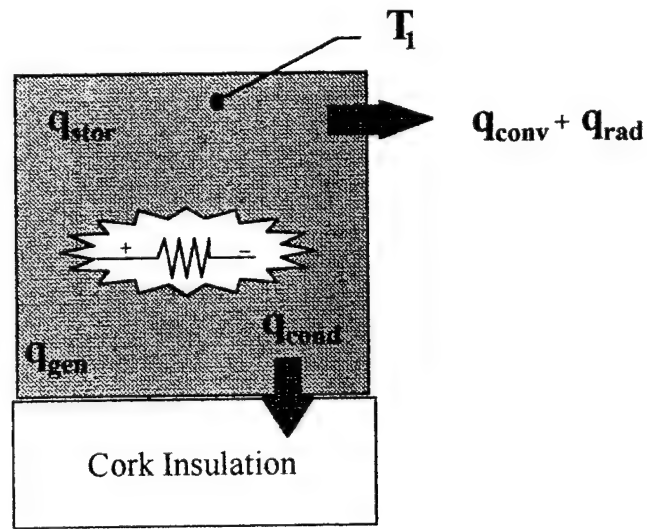


Figure 8. Simplified Model Temperature Response to a Sinusoid Heat Input

Thermal Control, Actual Model

The specific energy equation used in this research is represented by Equation (12) and can be derived from Figure 5 by removing the insulation from the top and sides. These modifications allow for convective and radiative heat losses. In addition, the conduction term is accounted for by allowing heat to transfer through the bottom surface. Figure 9 shows a representation of the actual model.



T_{∞} = Ambient Air Temp & Insulation Temp at the bottom of the insulation surface

Figure 9. Illustration of Actual Model & Control Volume

To simplify Equation (12), an analysis was performed to estimate the size of the different terms in the energy equation (see Appendix B). The analysis is believed to be slightly overestimated for the conduction mode, since the convection coefficient was assumed constant over all cork surfaces. In reality, the convection coefficient probably decreases near the cork base as the other components block the airflow. Nevertheless, the calculations suggest that at low speeds (2.2 m/s) the convective losses are at their lowest,

but the convection mode is still significantly larger than the other modes. It also suggests that as velocity increases, the losses due to conduction decrease. Table 2 gives a summary of the values at various speeds.

Table 2. Estimated Conductive Heat Losses for Different Operating Conditions

Velocity (m/s)	Surf Temp (C)	% Rad Loss	% Cond Loss	% Conv Loss
2.2	67.2	3	22	75
4.1	49.8	2	18	80
8.6	40.3	1	15	84
13.1	36.6	1	13	86
17.7	34.3	1	12	87
22.2	32.9	0.5	11.5	88
26.8	31.9	0.5	11	88.5

Based on the fact that temperatures were going to be regulated to values generally less than or equal to 40 deg C and that the conduction analysis was conservative, it was assumed that conductive losses would be less than 15%. Therefore, the heat generating surface touching the cork was assumed to be adiabatic. It should be noted that the conductive losses will act to make the effective heat generation rate in the control volume slightly less than the actual measured value (the adiabatic assumption will be revisited in Chapter 4).

Another simplification was achieved by maintaining low component temperatures. As mentioned earlier, radiation heat transfer is low at low temperatures. Estimated radiative losses for this thesis are tabulated for various conditions (with a heat generation rate of 3.39 watts) in Table 3. Total hemispherical emissivity values for copper are approximately 0.03 for highly polished surfaces and 0.5 for stably oxidized

surfaces [5]. The copper in this thesis was shiny, so emissivity was probably closer to the 0.03 value.

Table 3. Estimated Radiative Heat Losses for Different Operating Conditions

Surface Temp (C)	Ambient Temp (C)	Emissivity	Heat Loss (Watts)	% of Total Heat Loss
40	22	0.03	0.00533	0.16
40	22	0.5	0.08896	2.62
90	0	0.03	0.03113	0.92
90	0	0.5	0.51889	15.30
90	22	0.5	0.43018	12.68

Typical test conditions used in this study included ambient temperatures ranging from 19 to 22 deg C and surface temperatures ranging from 30 to 50 deg C. Heat generation rates were always constant at 3.39 watts. Since the radiation losses for these conditions were estimated to be very low, radiation was neglected. Finally, returning to Equation (12) and removing the conduction and radiation terms, the energy equation used in this research takes the form

$$-c\left(\frac{VL}{v}\right)_L^m \frac{k_f}{L} A(T_1 - T_\infty) + q_{\text{gen}} = \rho c_p V \frac{dT_1}{dt} \quad (24)$$

After letting C equal thermal capacitance and explicitly discretizing Equation (24), we have

$$T_1^{p+1} = T_1^p + \frac{q_{\text{gen}} \Delta t}{C} - \frac{c\left(\frac{VL}{v}\right)_L^m \frac{k_f}{L} A(T_1^p - T_\infty) \Delta t}{C} \quad (25)$$

Where T_1^i indicates T_1 at the i^{th} time step. This will be used in the simulation model.

III. EXPERIMENTAL & ANALYTICAL SET UP

Hardware Model Description

The actual hardware model consists of a 0.152 m inner diameter circular duct, a butterfly valve connected to a stepper motor, and a small electronic board with an electrical component that generates heat. A cut away illustration, Figure 10, shows the air inlet and the relative position of each component. The electrical component is illustrated in Figure 11. This assembly was positioned inside a wind tunnel.

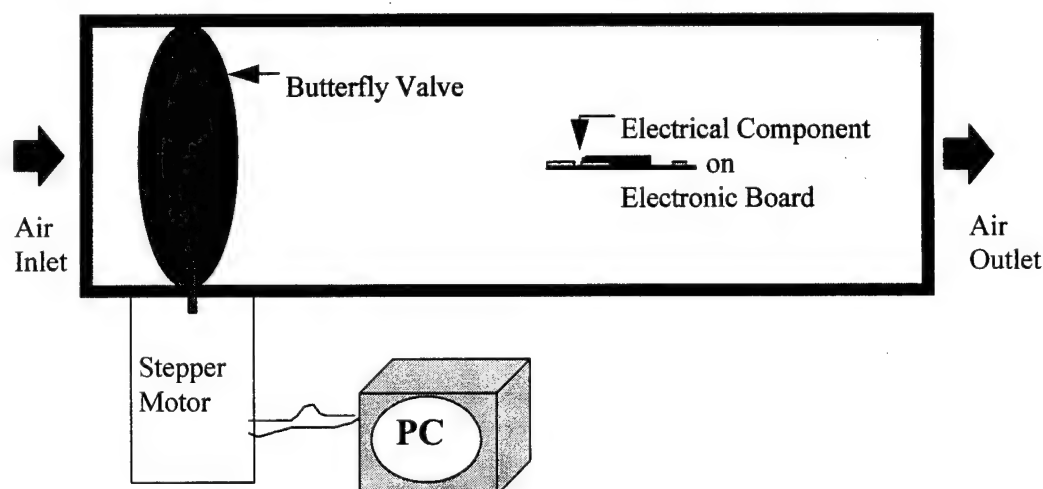
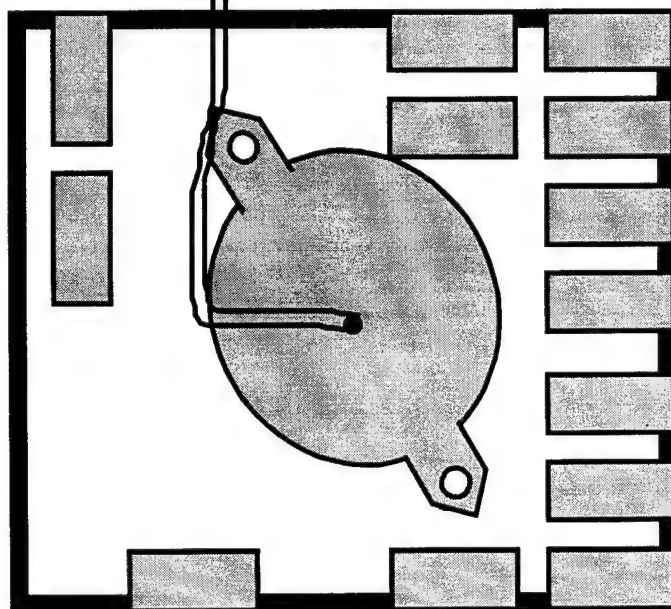
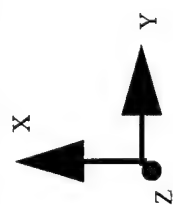
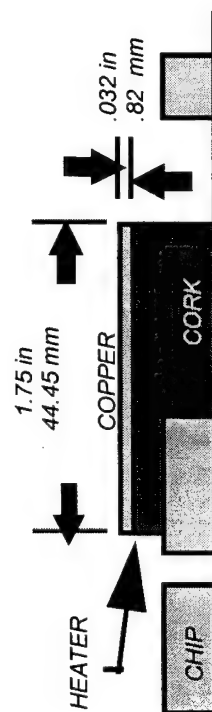


Figure 10. Illustration of Physical Model

Temperature regulation occurs by the PC-based controller operating on the error between the reference temperature and the measured temperature ($error = T_{ref} - T_1$). The measured temperature is obtained from a thermocouple mounted on the top center of the electrical component. The output of the controller is a pulse stream that is sent to the stepper motor. The stepper motor shaft rotates one step for every 5-volt pulse it receives. Each pulse corresponds to 360/4000 (0.09) degrees of shaft rotation. The rate of the pulses correspond to the angular velocity of the motor.



TOP VIEW (Approximate Size)



RIGHT SIDE VIEW (Approximate Size)



FRONT VIEW (Approximate Size)

Figure 11. Component Schematic

In addition, the sign of the error indicates the direction of motor travel. A positive value indicates that the measured temperature is less than the reference temperature so the motor should turn counter clockwise to close the butterfly valve. A negative value indicates that the measured temperature is greater than the reference temperature so the motor should turn clockwise to open the butterfly valve.

The freestream air is regulated to the test section by opening and closing the butterfly valve. The regulated test section air then flows over the component to increase or decrease the forced convection heat transfer rate.

Instrumentation

For one mode of operation, the only instrumentation required for this thermal control design was a temperature sensor (thermocouple) placed at the temperature regulation location. For more complex modes of operation, sensors were used to measure the freestream air temperature, component temperature, and freestream airspeed.

This study used pitot static tubes to measure velocities and T-type thermocouples to measure temperatures. All measured signals were amplified and the thermocouples were filtered to 10Hz before entering the data acquisition system (DAS).

Data Acquisition System

The digital data acquisition system consisted of three major components: a 486 PC, Lab View™ software, and an AT-MIO-16L software configurable data acquisition board from National Instruments Corp.® The software, Lab View™, is a graphical programming language for development of data acquisition and analysis applications. It is capable of providing complete control of the data acquisition board for sampling rate, gain, and input/output range. Features in the software also allow the user to change numerical variable values while the DAS is operating. This feature was used to set the reference temperature and controller gains.

The data acquisition board provided 12 bit analog to digital conversion (ADC) for up to 8 inputs in differential mode. In addition, it has two analog output ports and two digital ports (4 lines per port). The voltage range for both the input and output ports was set at ± 10.0 volts. The resolution of the board for this range was 4.88×10^{-3} volts.

The software performed two major tasks. First, it acquired and processed all the instrument signals. Second, it operated on the feedback error and controlled the stepper motor position. In the first task, the software acquired and converted each input signal to standard units. Thermocouple voltages were converted to degrees C and airspeeds were converted to m/s. These results were displayed on the monitor and stored in a buffer for retrieval. In the second task, the software compared the measured temperature signal to the user input reference temperature. The value of this error was decomposed into a magnitude and a sign. The magnitude and sign corresponded to a pulse stream and direction as described earlier in this chapter. Butterfly valve positions were limited to the

range of 0 degrees (closed) to 90 degrees (wide open) by a software subroutine. Acquire and command signals were updated at one second intervals.

In the software subroutine developed for this study, the controller output signal rate (motor pulses) could not be less than one pulse per second. To illustrate, if the controller gain was set at two and the error into the controller was 0.25 degrees C, the resulting signal out of the controller should be 0.5 pulses per second or one pulse every two seconds. Since the software subroutine was designed to read and write once a second, the signal from the controller (0.5 pulses per second) was over written with a value of one pulse per second. This characteristic becomes noticeable when low controller gains are used and when the system is in a steady state condition. A copy of the routine is included in Appendix C.

Simulation Model

MATLAB[®] SIMULINK[™] was the simulation program used to model the dynamic response of the system. SIMULINK[™] is a graphical modeling program that evaluates models in block diagram form. This program is extremely useful for control applications because many control models are arranged in input-output block diagram form. SIMULINK[™] allows the user to put algebraic or differential equations, as well as s-domain transfer functions, into modeled blocks.

Time responses from SIMULINK[™] models involve the numerical integration of ordinary differential equations. The integration algorithm used for this thesis was Linsim. The step size for each iteration was set to one second to match the hardware model's data acquisition and control step size [9].

As illustrated earlier, the actual hardware model was represented by a closed-loop negative unity feedback system modeled in block diagram form shown in Figure 12. Each block represents the modeled dynamics/characteristics of the hardware model.

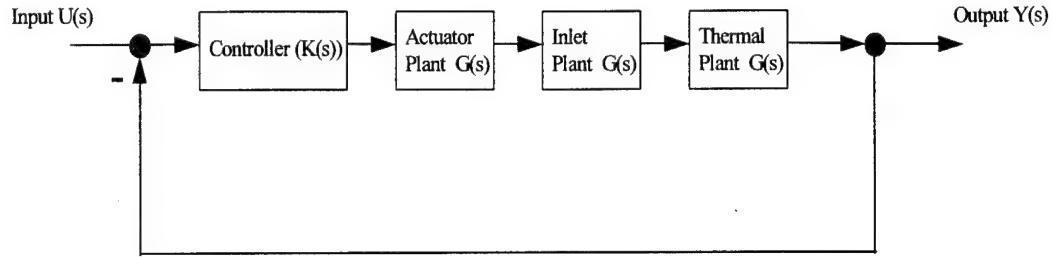


Figure 12. Illustration of the Closed-Loop Control Model

The actuator plant is a mathematical representation of the stepper motor. The dynamics that needed to be modeled from the stepper motor were the shaft's position. The input into the hardware stepper motor was a 5.0 volt pulse stream along with a high or low state for direction. The output was 0.09 degrees of clockwise shaft rotation for each pulse in the high state and 0.09 degrees of counterclockwise shaft rotation for each pulse in the low state. By integrating the pulse rate (angular velocity), the angular position of the shaft could be determined [10]. The derivation is

$$P = \text{Controller Output} = \frac{\text{Pulses}}{\text{Second}}$$

$$\dot{\theta} = \frac{d\theta}{dt} = -0.09 P$$

Converting to the s-domain

$$\begin{aligned} -0.09 P &= \theta s \\ \theta &= \frac{-0.09 P}{s} \end{aligned} \tag{26}$$

The SIMULINK™ simulation uses a limiting integration block to integrate the pulse rate and limit the range of shaft rotation between 0 - 90 degrees. An illustration of the actuator subroutine can be seen in Figure 13.

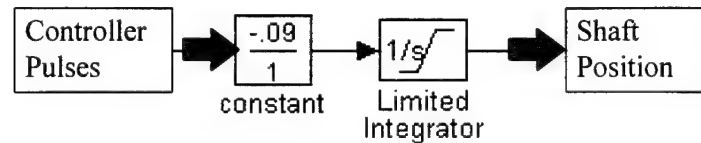


Figure 13. Illustration of the SIMULINK™ Actuator Plant

The inlet plant in Figure 12 is a mathematical representation of the butterfly valve. The characteristic that needed to be modeled from the butterfly valve was how it regulated the freestream airspeed to the test section airspeed. The actual test data that describes this characteristic will be presented in the section on component test results, while the modeled results will be presented now. First of all, between 0-28 degrees of butterfly valve travel, the test section velocity is due to leakage around the imperfectly sealed inlet. Between 28-90 degrees of butterfly valve travel, there is a nearly linear relationship between the inlet valve position and test section airspeed. An illustration of the modeled inlet characteristic is shown in Figure 14. The figure shows a plot of the test section airspeed (as a percentage of the constant freestream airspeed) against the inlet angle (leakage at 13%).

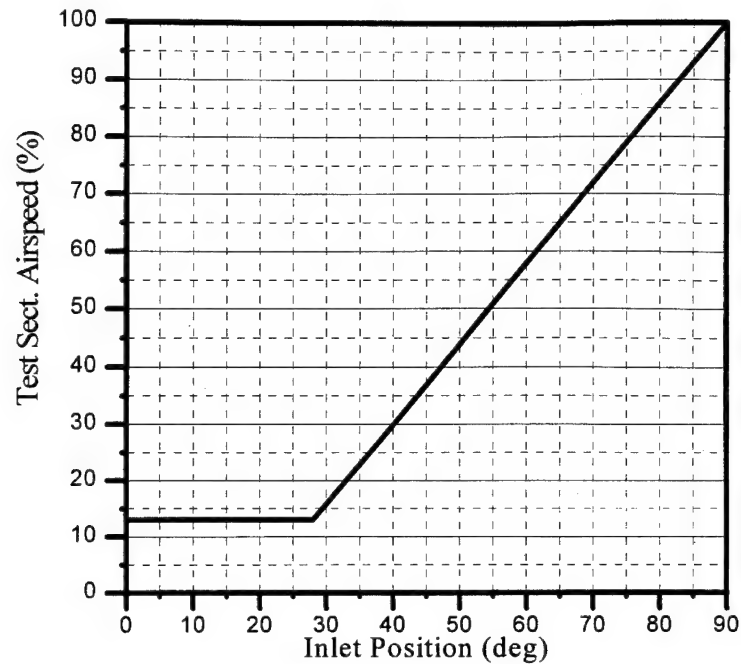


Figure 14. Illustration of Duct Inlet Curve

The SIMULINK™ representation of the inlet is shown in Figure 15. The inputs in this example are freestream airspeed (26.8m/s), inlet valve leakage (13%), and shaft position. The output is test section airspeed.

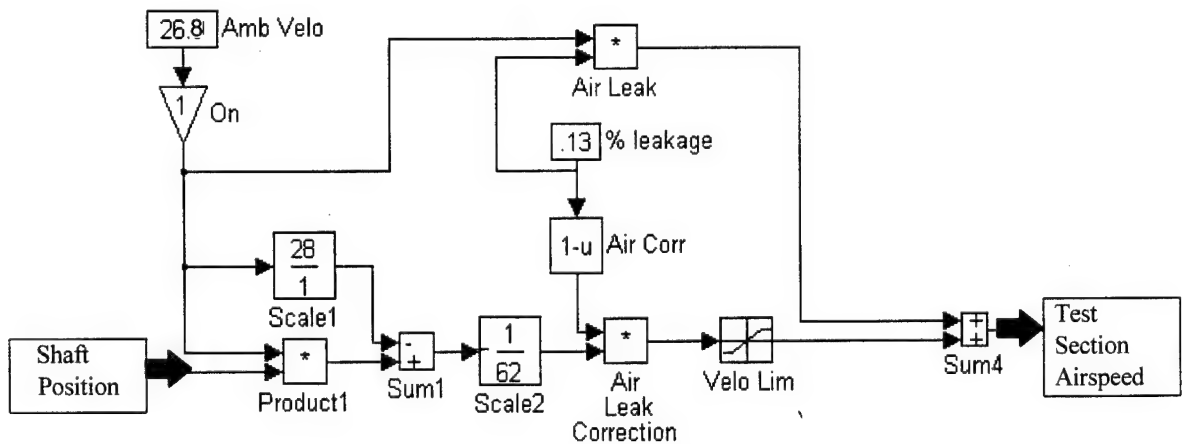


Figure 15. Illustration of the SIMULINK™ Inlet Plant

The thermal plant in Figure 12 is a mathematical representation of the electrical component. The characteristic that needed to be modeled was how the component temperature, at the thermocouple location, changed with varying test section airspeeds and with varying test section cooling air temperatures. The SIMULINK™ representation of the electrical component is shown in Figure 16. The simulated heat loss due to radiation was set to zero by assigning emissivity a value of zero. Inputs to the system are test section airspeed, ambient temperature, heat generation rate, Nusselt number, and thermal capacity. The output is component surface temperature.

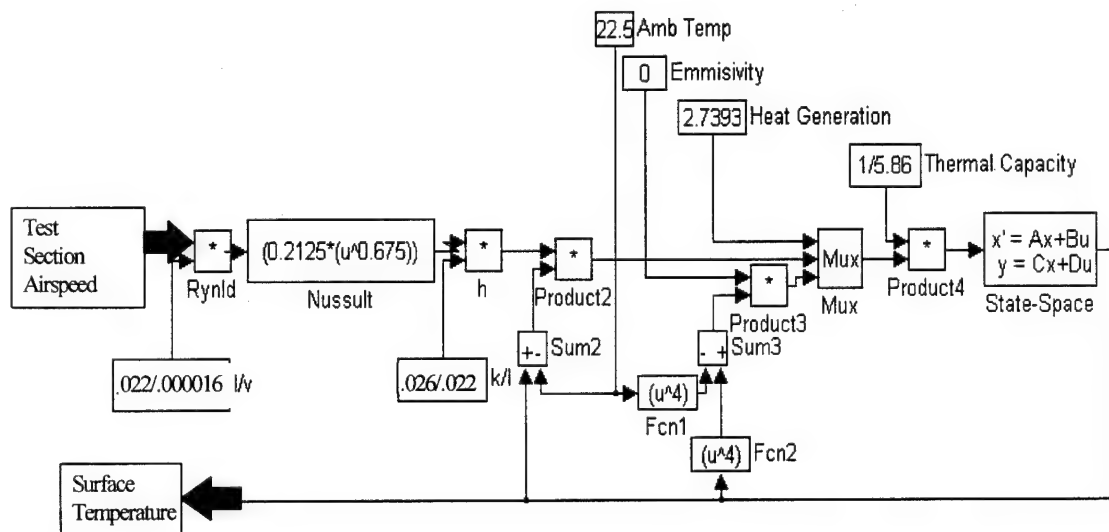


Figure 16. Illustration of the SIMULINK™ Thermal Plant

IV. RESULTS

Up to this point, the fundamental principles (Chapter II) and the hardware and simulation models (Chapter III) have been presented. The first part of this chapter supplements the section on the simulation model in Chapter III by presenting the actual data from the component tests. After presenting the component data, corrections to the simulation model are detailed. These corrections were made to improve the correlation between the simulation and hardware model results. This chapter then progresses into the controller design and evaluation. The controller design starts out simple by using a fixed proportional gain and comparing the simulation responses with experimental data. The fixed gain controller is then modified to be a scheduled proportional gain controller that was obtained with least squares techniques. Next, the system is linearized and root locus techniques are used to design a proportional-derivative (PD) controller. The PD controller gets optimized to a proportional-integral-derivative (PID) design with the help of MATLAB[®]'s Nonlinear Controller Design (NCD) Toolbox. Lastly, to compare the simulation responses to experimental data for an advanced PID controller, an advanced PID controller was run on the simulation and experimentally.

Component Test Results

To start out, the uncertainty associated with the measurements in this study can be seen in Table 4.

Table 4. Measurement Uncertainty

Measurement	Uncertainty
Temperature	± 1 deg C
Airspeed (< 8 m/s)	± 1 m/s
Airspeed (< 22 m/s, >8 m/s)	± 0.75 m/s
Airspeed (> 22 m/s)	± 0.5 m/s
Orientation	± 1 deg
Mass	± 0.0001 kg
Length	± 0.001 m
Voltage	± 0.02 v
Ampere	± 0.002 amps

The inlet plant data was obtained by performing a series of tests that varied the freestream airspeed and butterfly valve angle while recording the test section airspeed. Specifically, pitot static tubes were fixed in the freestream air and test section. The test section pitot static tube was placed in the location of the electric component. The freestream airspeed was held constant and the butterfly valve was opened in nine degree increments. At each increment, the test section pitot static tube value was recorded. This process was repeated for seven different freestream airspeeds. The results are shown in Figure 17 (see Appendix D for a detailed explanation of this test). Even though the data also indicated that there was no airflow in the test section when the valve was in the range of 0-28 degrees, it was determined that some inlet leakage was actually present. This was determined by placing the thermocoupled component in the test section, closing the inlet, and adjusting the freestream airspeed. It was observed that as the freestream airspeed

increased, the steady state component temperature decreased. It was believed that when the valve was in the range of 0-28 degrees, the pitot tube was in a location where low speed, irregular airflow was present (air not flowing axially through the duct). Therefore, the pitot tube was not capable of sensing the flow. The next section (Hardware and Simulation Model Correlation) will quantify the air flow in the 0-28 degree region.

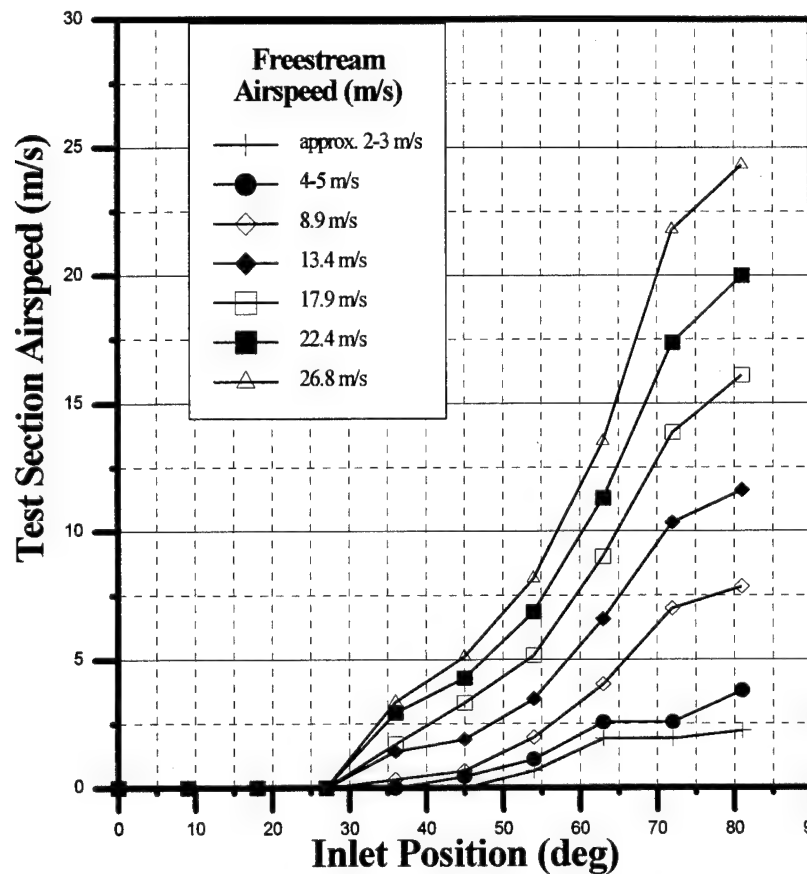


Figure 17. Family of Curves for the Inlet Model

The next series of tests was performed to understand the cooling characteristics of the electric component. The first test varied the orientation of the component in the freestream air. The purpose of this test was to determine the orientation of the component

that maximized the convective heat transfer losses. In this test, the freestream airspeed was fixed and the component orientation was varied in 30-degree increments from 0 degrees to 180 degrees. At 180 degrees (Figure 18, Position A) the component board was in a vertical position with the heated electric component on the back side. At 90 degrees (Figure 18, Position B) the component board was in a horizontal position with the heated electric component facing up. At 0 degrees (Figure 18, Position C) the board was vertical again, this time with the electric component facing the oncoming air.

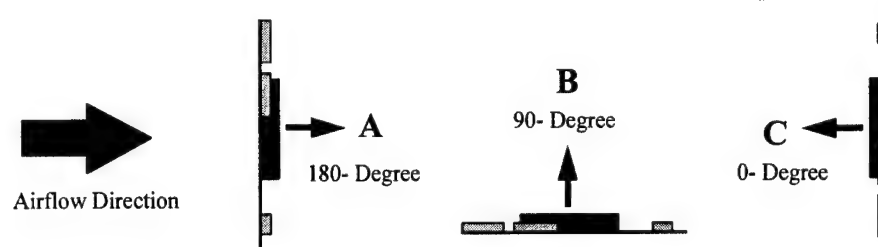


Figure 18. Illustration of Component Orientation

The data in Figure 19 indicates that the 90-degree position maximizes the component's forced convection heat losses. Based on this data, the component was fixed in the 90-degree position for all other tests (see Appendix E for a detailed explanation of this test).

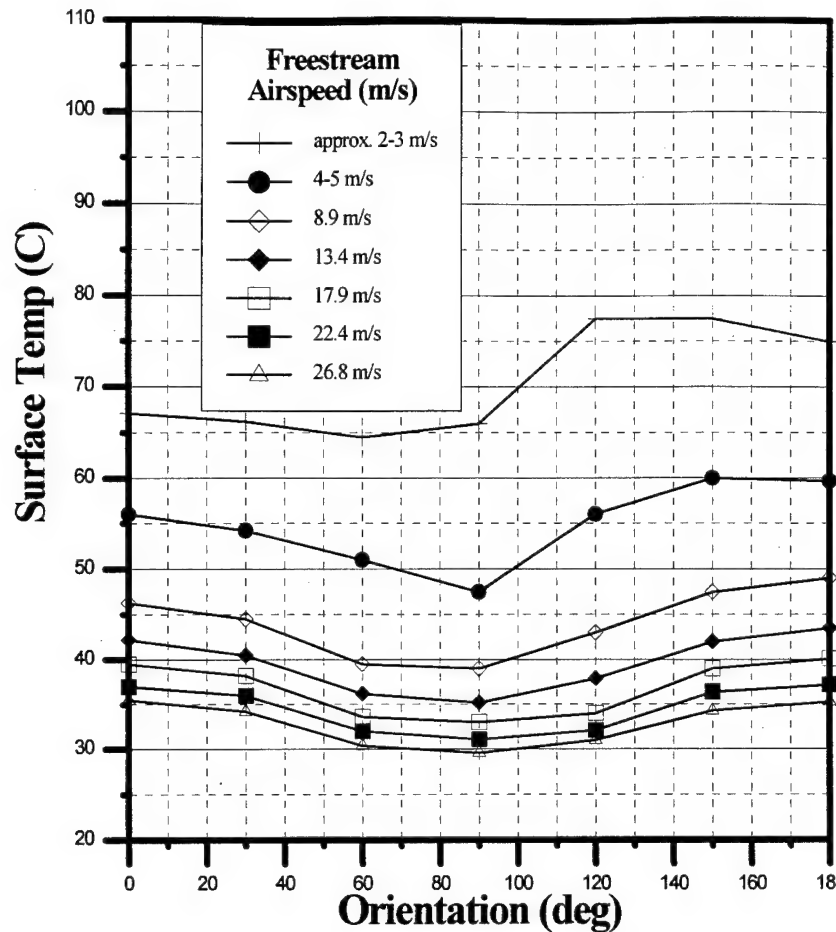


Figure 19. Surface Temperature vs. Component Orientation Test Data

The next component test was performed to determine the Nusselt number as a function of cooling airspeed. This was accomplished by evaluating Equation (24) at steady state conditions. The electrical component contains a thin-film resistance heater that was turned on and held at a constant heat generation rate of 3.39 watts. With surface area, surface temperature, and ambient temperature known, the convection coefficient was calculated. By knowing the convection coefficient at an airspeed, the value of the Nusselt number for that airspeed was obtained. By using Equation (11) and plotting log Nusselt number vs. log Reynolds number, the constants c and m were determined with a first order

least squares curve fit. For the three runs, $Nu_{L,1} = 0.21 Re^{0.67}$, $Nu_{L,2} = 0.26 Re^{0.64}$, and $Nu_{L,3} = 0.28 Re^{0.64}$. Figure 20 shows the data from the three runs along with a line representing the mean value of the Nusselt number ($c = \text{mean } 0.25$ with std. dev. ± 0.036 , $m = \text{mean } 0.65$ with std. dev. ± 0.017) and a line representing the Nusselt number used in the simulation ($c = 0.2125$, $m = 0.675$) (air properties evaluated at T_{film} -see Appendix F for a detailed explanation of this test).

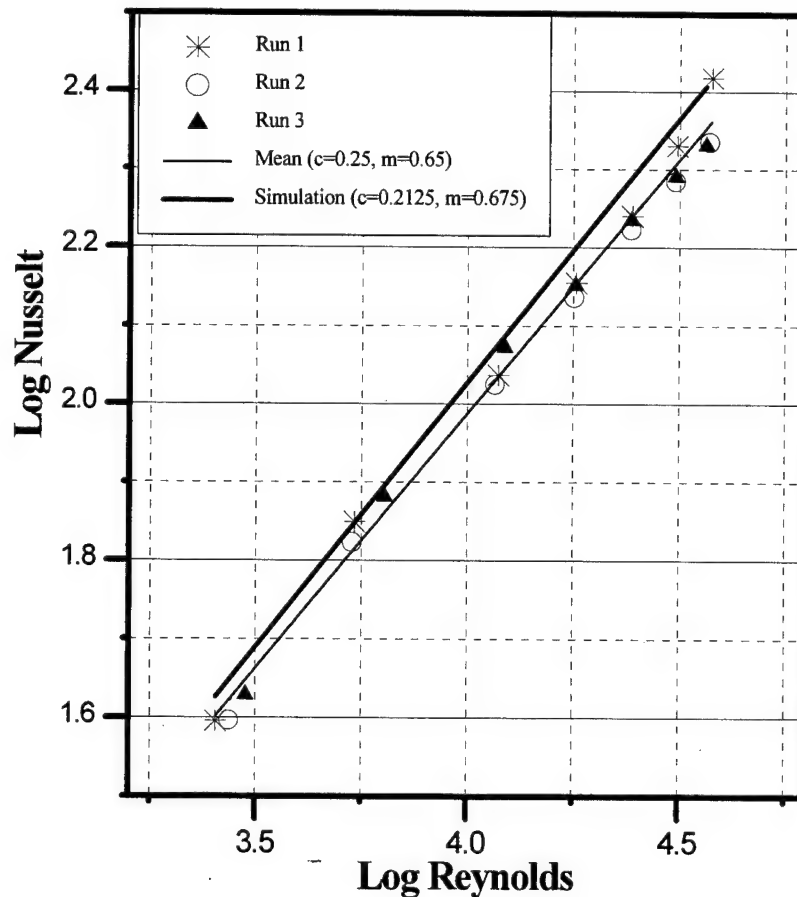


Figure 20. Dimensionless Representation of Heat Transfer Coefficient

Hardware & Simulation Model Correlation

As stated earlier, this section will explain the corrections that were made to the simulation model to enable its performance to more closely match the actual hardware's performance. Note, this study did not limit the model adjustments to the mean values of the measured data. To get the best possible simulation-hardware performance correlation, refinements had to be made to both the inlet and thermal simulation models.

One refinement was made to the inlet model. This refinement was required to account for the convective heat losses that occurred when freestream air leaked past the closed inlet. In addition, it also accounts for the poor test section airflow measurements in the 0-28 degree range. As mentioned in Chapter III, this leakage was modeled in the simulation as a percentage of the freestream airspeed. The value of 13% was determined by matching hardware data to simulation data when the inlet was in the closed position. To illustrate the matching process, when the value of 10% was placed in the simulation model with a closed inlet, the transient and steady state temperatures from the simulation were too large relative to the closed inlet test data. This indicated that the modeled convective losses were too low. When the value of 15 % was placed in the simulation model, the transient and steady state temperatures from the simulation were too low relative to the test data. This indicated that the modeled convective losses were too high. The value of 13% gave the best match to the test data where freestream airspeeds were 8.9 m/s, 17.9 m/s, and 26.8 m/s. These results are shown in Figure 21.

The leakage value of 13% can be checked by evaluating the data from the three Nusselt number runs in Figure 20 and the three steady state component temperatures in Figure 21. Figure 22 shows the seven data points for each Nusselt number run and the

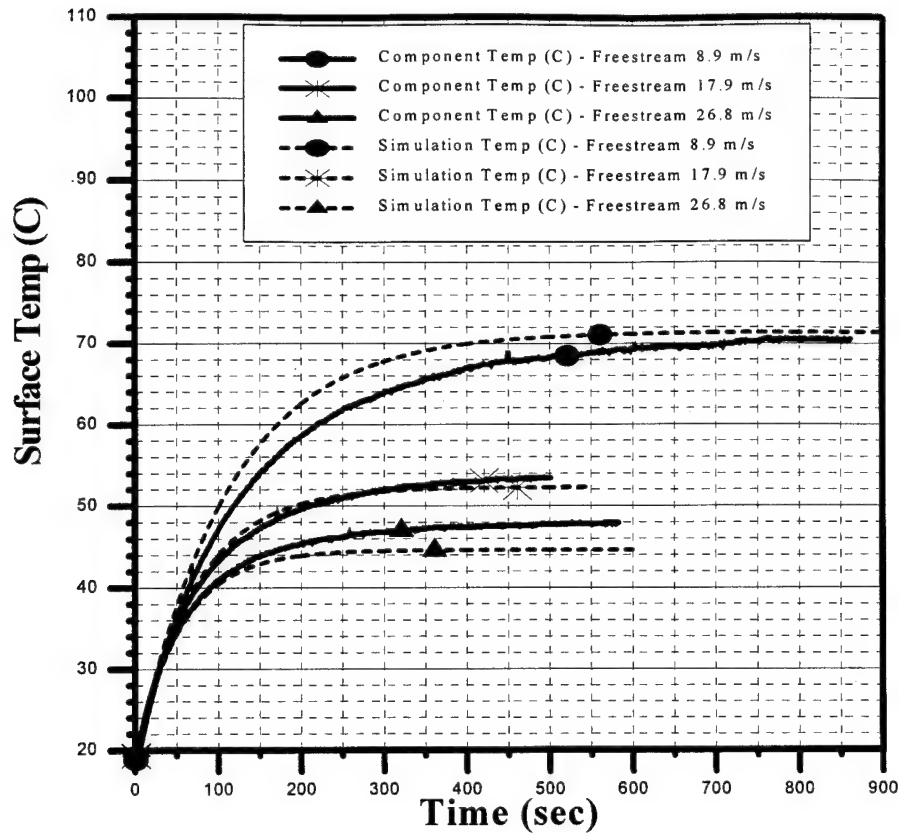


Figure 21. Inlet Leakage Correlation

three component data points from the leakage test. The three component data points from the leakage test correspond to the estimated steady state component temperatures of 48, 54, and 70 deg C (from Figure 21) and airspeeds of 3.5, 2.3, and 1.2 m/s (13% of the freestream airspeed values 26.8, 17.9, and 8.9 m/s, respectively). In short, the three component data points with airspeed values of 13% (plotted in Figure 22), follow the trend established by the Nusselt number data. To illustrate a poor match, if the leakage was modeled at 25% of the freestream airspeed, the data points would be placed at 48 deg C vs 6.7 m/s, 54 deg C vs 5 m/s, and 70 deg C vs 2.25 m/s. These points would not follow the trend established by the Nusselt number data.

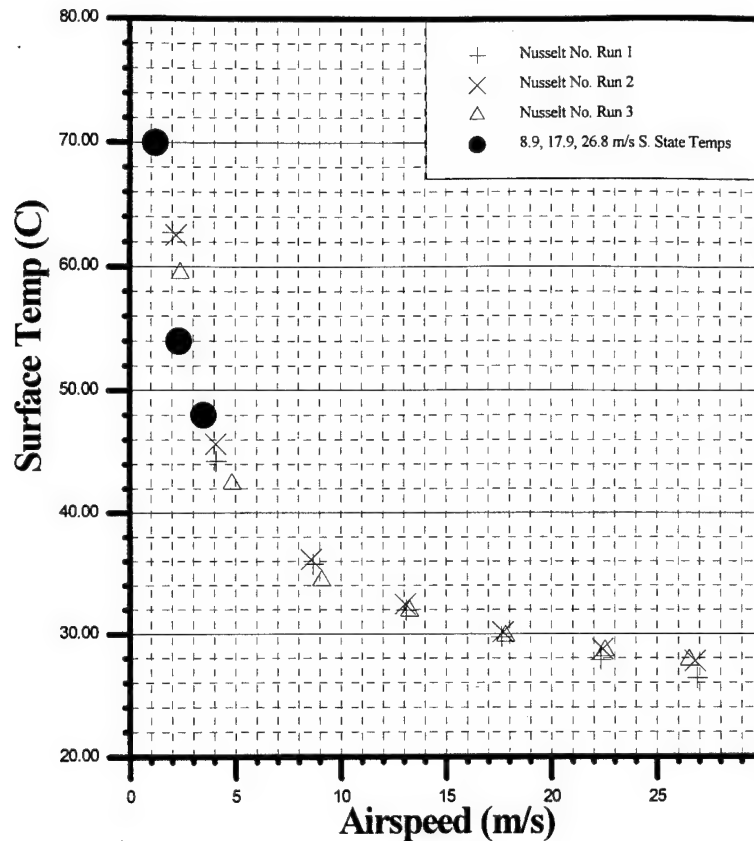


Figure 22. 13% Leakage Verification Plot

Three refinements were made to the thermal plant. They were made to the heat generation rate, the thermal capacity, and the Nusselt number. The refinements to the heat generation rate and thermal capacity were accomplished simultaneously and they were the result of the simplifying adiabatic assumption made in Equation (24). In Equation (24) it was assumed that there were small conductive losses to the cork insulation so the surface touching the cork was treated as adiabatic. The adiabatic assumption leads to a slight simulation response error. To correct this error, and to account for small conductive losses, the measured energy generation value of 3.39 watts was reduced to 2.74 watts.

Clearly, it is difficult to predict the exact contribution of each heat transfer mode and the exact thermal capacitance of the electric component. Nevertheless, by examining Equation (24) with test section airspeed set to zero, a close approximation of the ratio of heat generation rate to thermal capacity could be obtained. Figure 23 shows the component heat-up profile with no forced convection cooling, and it also shows the slope of this heat-up profile over the first 30 seconds.

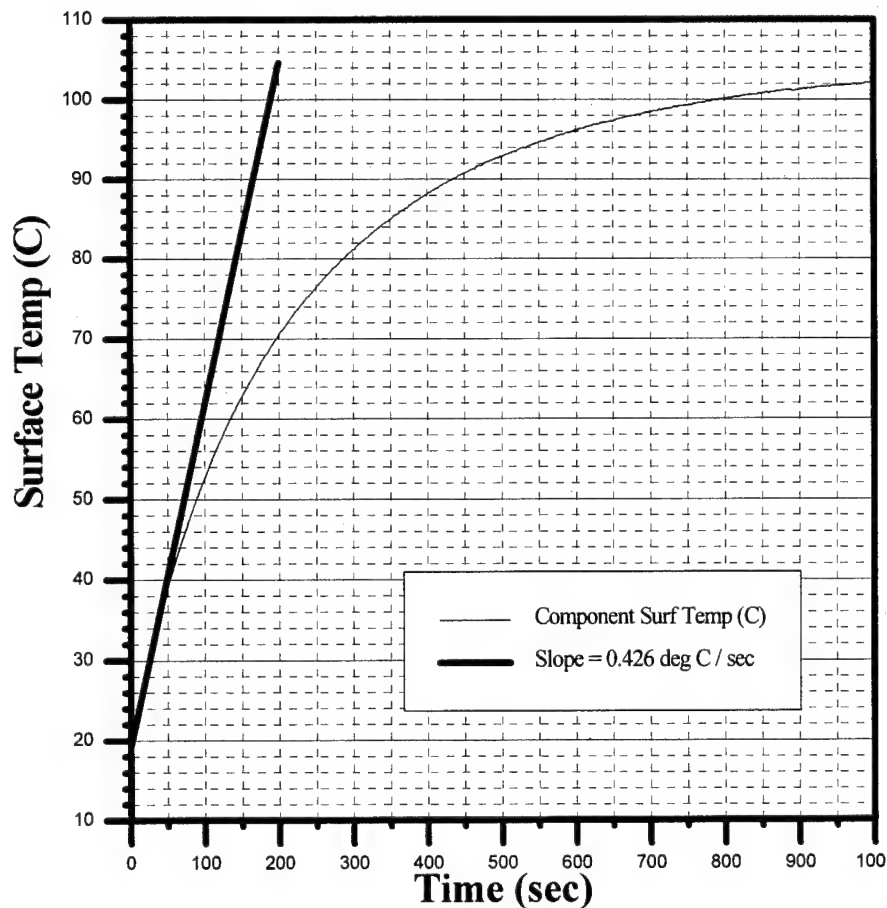


Figure 23. Actual Heat Generation Rate to Thermal Capacity Ratio

The actual measured power into the component heater was 3.39 watts. The thermal capacity of the control volume was 5.67 J / deg C (copper plate - 4.88 J / deg C, heater - 0.79 J / deg C). These values provide a heat rate to thermal capacity ratio of 0.60 deg C / sec. The slope from Figure 23 was 0.426 deg C / sec. The simulation was simply adjusted by iteratively dropping the heat generation rate from 3.39 watts to 2.74 watts and increasing the thermal capacity from 5.67 J / deg C to 5.86 J / deg C. This caused the simulation's heat rate to thermal capacity ratio to equal 0.467 deg C / sec, more closely approximating the slope in Figure 23. These adjustments resulted in a 19.2% drop in the heat generation rate and a 3.4% increase in thermal capacity.

The last refinement was made to the Nusselt number. The values of c and m were adjusted to tune the inlet response. The values of c (0.25 ± 0.036) and m (0.65 ± 0.017) that were empirically determined were slightly offset from the mean values for the simulation to $c = 0.2125$ and $m = 0.675$. The simulation values of c and m had standard deviations of 1.05 and 1.47, respectively. Examples of the correlated models will follow in the next section.

These adjustments deserve further discussion. When the correlating adjustments were initially made, they were based on insight that was obtained during the preliminary control volume calculations and experimental runs. It seemed obvious that some cooling airflow was present when the inlet was closed, the control volume was not perfectly insulated, and the empirical Nusselt number was not exactly equal to the mean values in the simulation. As a result, by accounting for the leakage, adjusting the heat generation and thermal capacity, and slightly modifying the Nusselt number, the simulation responses

could more closely approximate the actual hardware responses. After further evaluating the adjustments, it was determined that they could be supported with more scientific rationale. The data in Figures in 21, 22 and 23 provide some of the support. More support can be made by going back to Chapter 2. In that chapter, the control volume was defined as the copper plate and the heater. Therefore, adjustments to the thermal capacity can be justified if they are associated with the mass and the specific heat values of the copper plate and heater. The thermal capacity was only increased 3.4%. Also, for this same control volume, the heat generation rate probably does not equal the full measured 3.39 watts because the surface touching the cork is not perfectly adiabatic. As a result, when the heater was immediately turned on, some thermal energy immediately flowed into the nearby cork, which is not in the control volume. The heat generation rate was reduced 19.2%. From this perspective of the control volume, the original pin fin calculations that were done to estimate conduction losses (Table 2) appear to be fairly accurate.

Proportional Controller Design

With the simulation model correlated, the temperature regulating capabilities of a proportional controller were evaluated. There were two aspects to this evaluation. The first was to understand how the system regulated temperature and used inlet control when the freestream airspeed and the difference between the reference temperature and ambient temperature were varied. The second aspect was to develop an algorithm that would schedule the proportional gain to keep temperature responses within a desired performance range when the airspeed and temperature difference (T_{diff}) parameters changed.

The first aspect of this section was accomplished by making 27 runs with variations in the gain, airspeed, and temperature difference. There were three variations in airspeed and three variations in temperature difference (at each airspeed) for a total of nine test conditions. At each of these nine conditions, gain was varied with values of 0.5, 2.0, and 8.0. Table 5 shows the specific values for the nine test conditions.

Table 5. Test Condition Values

Condition	Freestream Airspeed (m/s)	Temperature Difference (C)	Reference Temperature (C)
1	8.9	16	35
2	8.9	21	40
3	8.9	31	50
4	17.9	15	35
5	17.9	20	40
6	17.9	30	50
7	26.9	10	30
8	26.9	15	35
9	26.9	20	40

Figure 24 shows the simulation and hardware, temperature and inlet position responses, for Condition 1 in Table 5, with a gain of 0.5. For the hardware response, there is a large temperature overshoot of 40%, with little control usage. Figure 25 shows the responses (temperature and inlet position) at the same condition (Condition 1 in Table 5) with a gain of 8.0. For the hardware response, the temperature overshoot is much smaller (16%), but the control usage is much greater. Figures 24 and 25 both show that the simulation and hardware models are well correlated at Condition 1. Figure 26 shows the simulation and hardware responses for Condition 3 in Table 5, with a gain of 8.0. This condition has a large temperature difference (31 deg C) and a hardware temperature overshoot of 6%. Notice that the temperature is very strongly regulated with a lot of control usage and that the simulation responses correlate well with the hardware responses. Figure 27 shows the simulation and hardware responses for Condition 8 in Table 5, with a gain of 8.0. This condition has a freestream airspeed of 26.8 m/s and the gain is just about right for a temperature overshoot of about 10%. Also, there is a fair amount of control usage and the steady state value for the inlet did not match as well to the hardware response. The poor match is the result of inaccuracies in the inlet model. The simulation allows too much airflow at the knee of the curve shown in Figure 14.

After evaluating the temperature responses at the nine conditions in Table 5 it was concluded that it was not possible to guarantee a single temperature response with one fixed proportional gain. Just by looking at Conditions 1 (Figure 24) and 6 (not shown), with a gain of 0.5, the temperature overshoot varied by 40%.

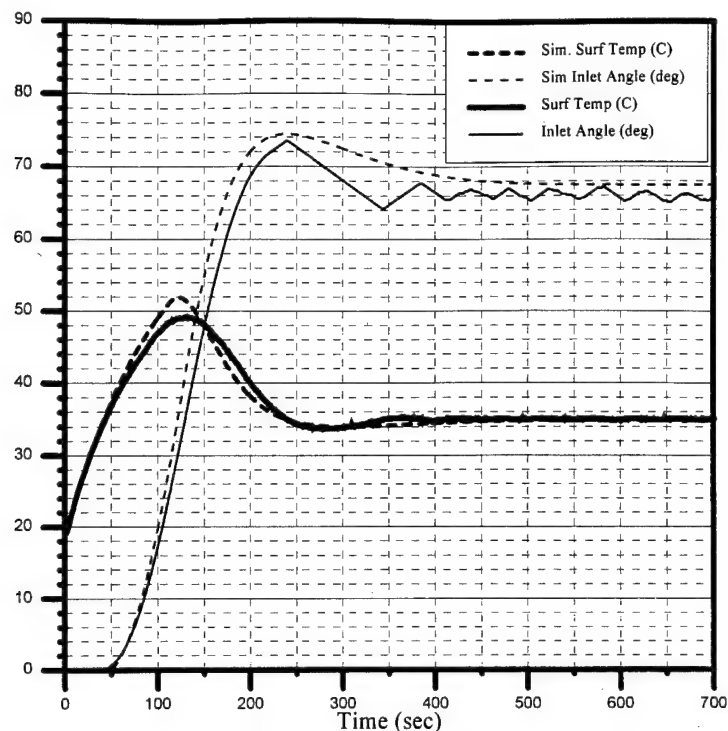


Figure 24. Comparison of Simulation and Hardware Model Responses
Condition 1, Gain-0.5, Ref Temp-35(C), Freestream Airspeed-8.9(m/s)

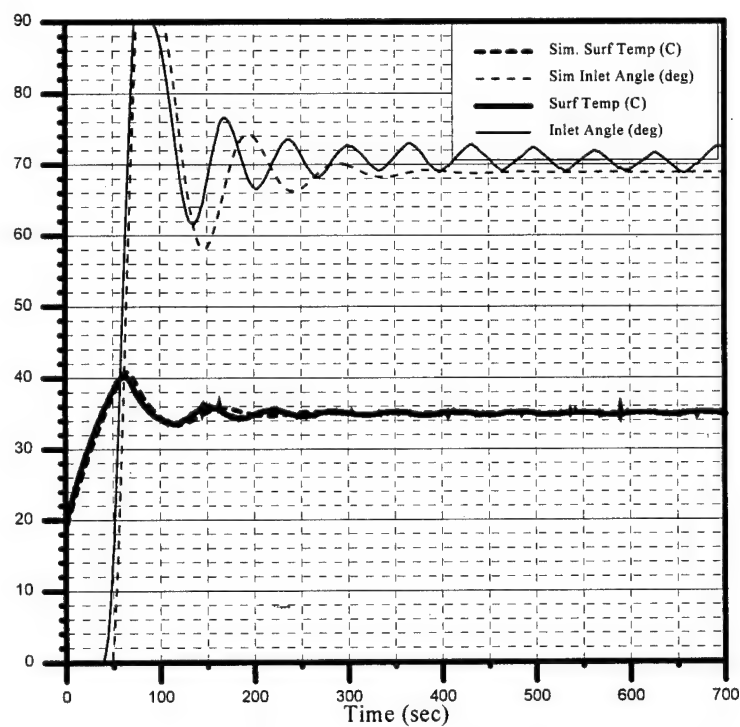
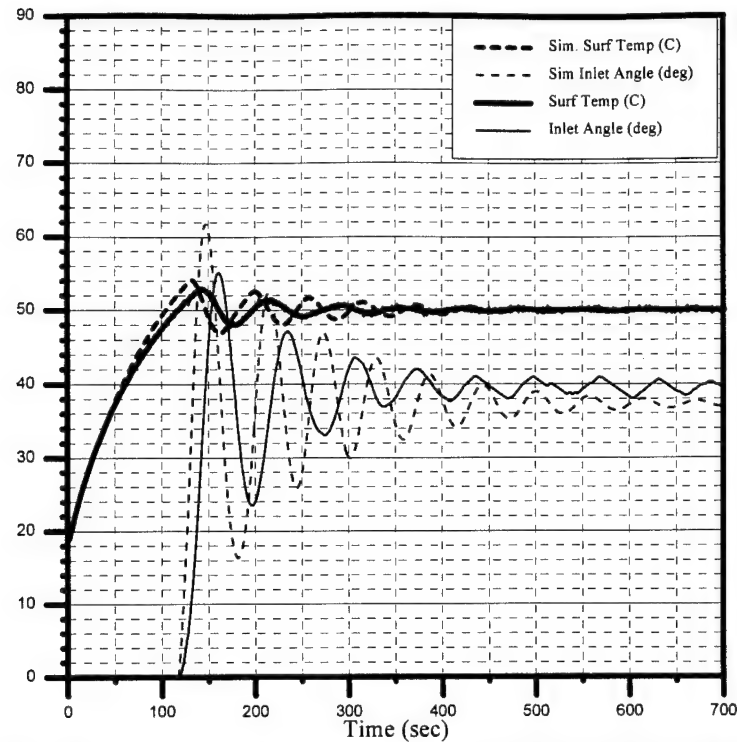
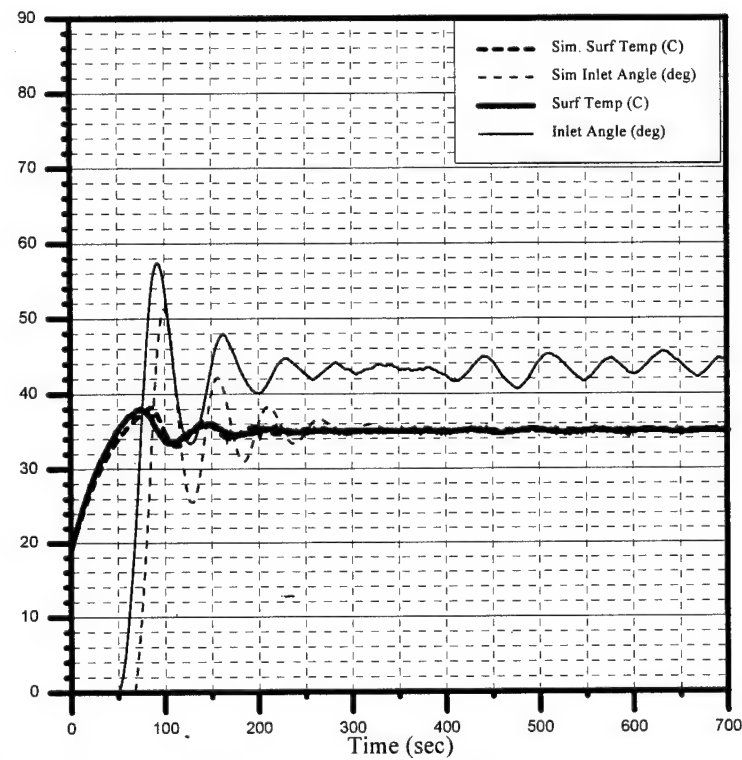


Figure 25. Comparison of Simulation and Hardware Model Responses
Condition 1, Gain-8, Ref Temp-35(C), Freestream Airspeed-8.9(m/s)



**Figure 26. Comparison of Simulation and Hardware Model Responses
Condition 3, Gain-8, Ref Temp-50(C), Freestream Airspeed-8.9(m/s)**



**Figure 27. Comparison of Simulation and Hardware Model Responses
Condition 8, Gain-8, Ref Temp-35(C), Freestream Airspeed-26.8(m/s)**

Based on the poor temperature regulating performance with the fixed proportional controller, a variable proportional controller was developed. By knowing that the freestream airspeed and the temperature difference affected the convection heat loss rate, a gain schedule based on these two variables was developed.

The mathematical tool used to generate the algorithm was the least squares method, using data from the 27 runs just discussed. From this data, an attempt was made at keeping the maximum overshoot temperature within 10% of the reference temperature. At each of the nine conditions in Table 5, a gain was approximated by evaluating the temperature responses that were generated by the three gains.

By plotting the values of airspeed, temperature difference, and gain at each of the nine conditions (see Table 6), it appeared that the gain values varied in a second order nature with both airspeed and temperature difference. Using the least squares methods, the scheduled gain can be expressed as a second order function of both airspeed and temperature difference as

$$Gain = 47.45 - (0.8767 \times T_{diff}) - (0.0032 \times T_{diff}^2) - (1.600 \times V_{\infty}) + (0.0223 \times V_{\infty}^2) \quad (27)$$

An important point to recognize is the increased complexity of this temperature control system. With the fixed proportional controller, only one thermocouple on the electric component was required. For the scheduled proportional controller, the same component mounted thermocouple was required, but additional sensors are required to measure cooling air temperature and freestream airspeed.

Table 6. Scheduled Proportional Controller Data

Condition	Freestream Airspeed (m/s)	Temperature Difference (C)	Estimated Gain
1	8.9	16	30
2	8.9	21	8
3	8.9	31	2
4	17.9	15	9
5	17.9	20	6
6	17.9	30	1
7	26.8	10	10
8	26.8	15	6
9	26.8	20	4

A projection of Equation (27) is shown in Figure 28. The three test conditions (Conditions 1, 3, and 8) that were shown previously were rerun on the simulation model to review the temperature response with the scheduled controller values (this controller was not tested with an experimental run). However, Figure 29 shows the simulation responses for Condition 1 when the scheduled gain of 20.14 was used. For the simulation, the temperature overshoot was 11%, which was slightly greater than the 10% objective. Figure 30 shows the simulation responses for Condition 3 when the scheduled gain of 4.72 was used. The temperature overshoot achieved the desired 10% objective. Figure 31 shows the simulation responses for Condition 8 when the scheduled gain of 6.72 was used. Again, the temperature overshoot achieved the 10% objective.

An observation from this evaluation was that a scheduled proportional controller based on the least squares algorithm did keep the temperature response close to the performance objective. It also required increased hardware complexity due to the added sensors.

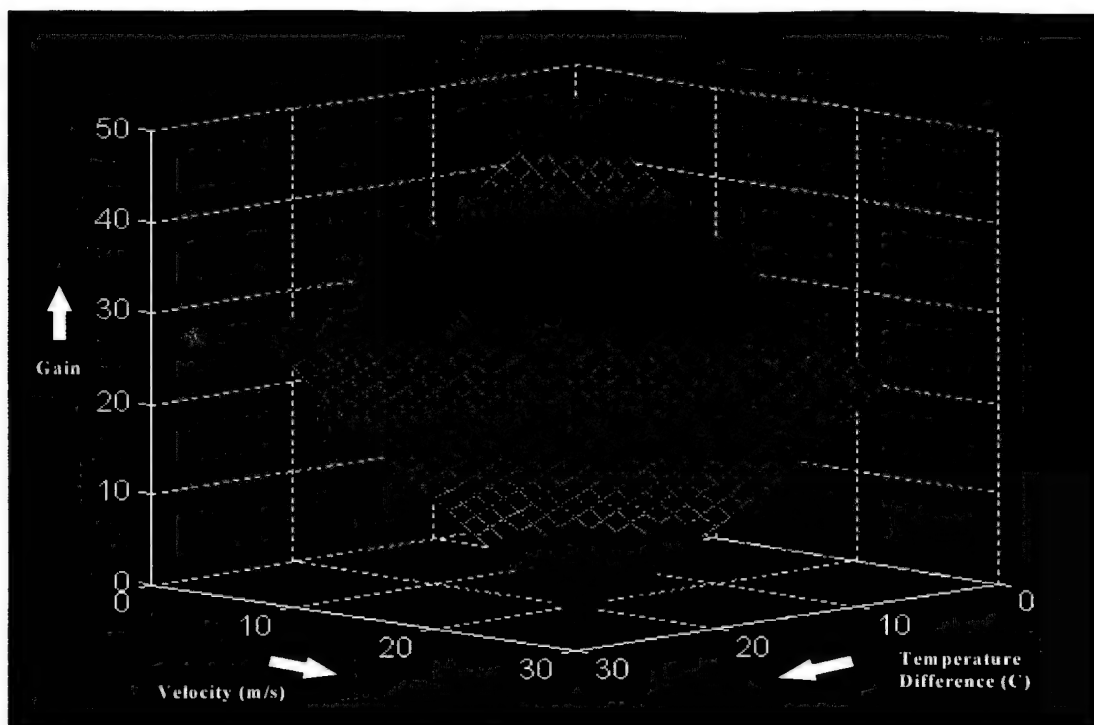


Figure 28. Gain Values for the Scheduled Proportional Controller

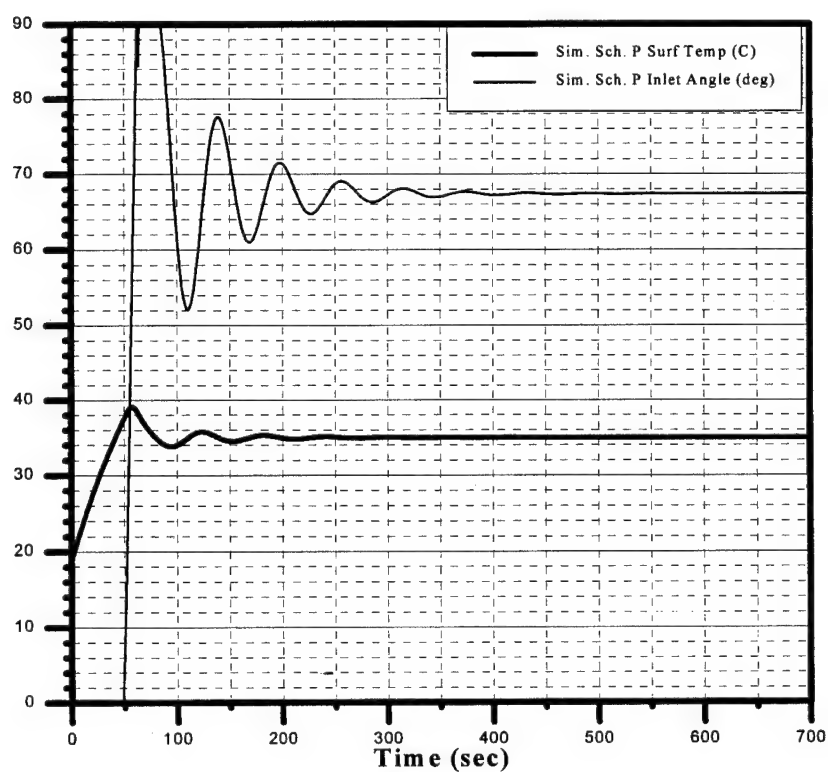
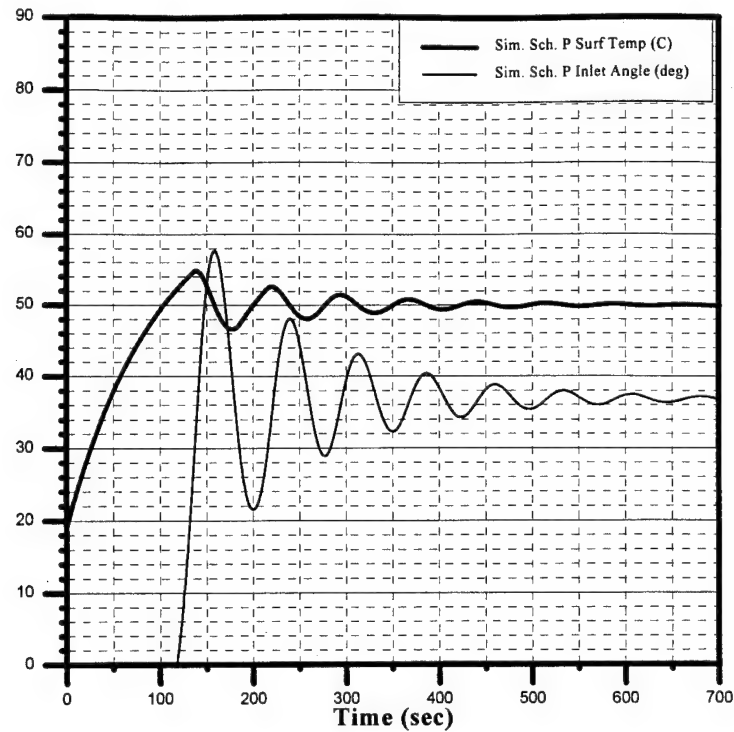
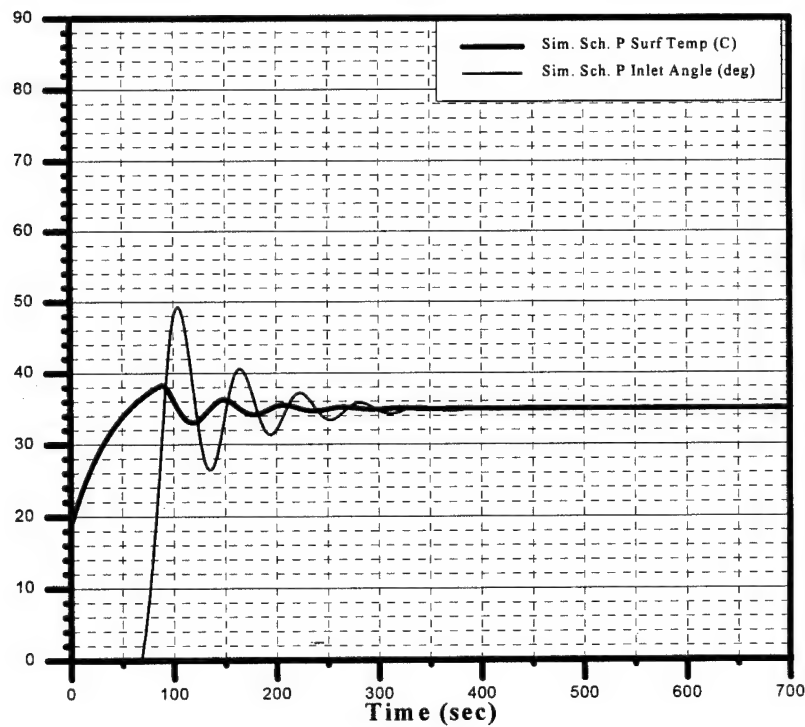


Figure 29. Condition 1, Scheduled Gain-20.14, Ref Temp-35(C), Freestream Airspeed-8.9(m/s)



**Figure 30. Condition 3, Scheduled Gain-4.72, Ref Temp-50(C),
Freestream Airspeed-8.9(m/s)**



**Figure 31. Condition 8, Scheduled Gain-6.72, Ref Temp-35(C),
Freestream Airspeed-26.8(m/s)**

Linearized Plant & Root Locus Controller Design

The proportional controller designs in the previous section did regulate temperatures to the reference values, and by using the scheduled controller there was some performance control when either the freestream airspeed or the temperature difference changed. However, the proportional controller designs tend to have responses that oscillate before achieving their steady state values. Unfortunately, to design a controller that is more advanced (than the proportional controller) and capable of reducing the oscillations, the design tools and techniques usually require linearized plants. In this section, the system will be linearized and a root locus diagram will be used to design a controller. The proportional-derivative (PD) controller that is designed in this section shows significant improvements over the simple proportional controller.

The first task in this control design was to obtain a linearized model of the system. To start out, a first order Taylor series expansion was performed on Equation (24). With the thermal plant linearized, the inlet and motor plants were combined to form a single linear system plant. The linearization steps are shown below.

Expand and rearrange Equation (24) to get

$$-cV^m \left(\frac{L}{v} \right)_L^m \frac{k_f}{L} AT_1 + cV^m \left(\frac{L}{v} \right)_L^m \frac{k_f}{L} AT_\infty + q_{\text{gen}} - \rho c_p V \frac{dT_1}{dt} = 0 \quad (28)$$

Since $f(V) = f(V_o + \Delta V) = f(V_o) + f'(V_o)\Delta V$ we have $V^m = V_o^m + mV_o^{m-1}\Delta$ and

$T_1 = T_{1o} + \Delta T_1$. After substituting, canceling out the nominal point and nonlinear terms, and converting to the s-domain, we get

$$\begin{aligned}
& -cV_o^m \left(\frac{L}{v} \right)_L^m \frac{k_f}{L} A \Delta T_1 + cV_o^m \left(\frac{L}{v} \right)_L^m \frac{k_f}{L} A T_\infty + cmV_o^{m-1} \Delta V \left(\frac{L}{v} \right)_L^m \frac{k_f}{L} A T_\infty \\
& - cmV_o^{m-1} \Delta V \left(\frac{L}{v} \right)_L^m \frac{k_f}{L} A T_{1o} - \rho c_p V \Delta T_1 s = 0
\end{aligned} \tag{29}$$

Rewriting the thermal plant in input output format for the change in surface temperature with small changes in test section velocity produces

$$\frac{\Delta T_1(s)}{\Delta V(s)} = \frac{cmV_o^{m-1} \left(\frac{L}{v} \right)_L^m \frac{k_f}{L} A (T_\infty - T_{1o})}{\rho c_p V s + cV_o^m \left(\frac{L}{v} \right)_L^m \frac{k_f}{L} A} \tag{30}$$

Next, the thermal plant needs to be combined with the inlet plant and the actuator plant. The linear region of the inlet valve can be approximated by

$$\frac{\Delta V(s)}{\Delta \theta(s)} = \frac{V_\infty}{62} \quad \text{Inlet Plant} \tag{31}$$

Thus,

$$\frac{\Delta T_1(s)}{\Delta \theta(s)} = \frac{cmV_o^{m-1} \left(\frac{L}{v} \right)_L^m \frac{k_f}{L} A (T_\infty - T_{1o})}{\rho c_p V s + cV_o^m \left(\frac{L}{v} \right)_L^m \frac{k_f}{L} A} \times \frac{V_\infty}{62} \tag{32}$$

Next we have

$$\frac{\Delta \theta(s)}{\Delta P(s)} = -\frac{0.09}{s} \quad \text{Actuator Plant} \tag{33}$$

So that

$$\frac{\Delta T_1(s)}{\Delta P(s)} = \frac{-cmV_o^{m-1}\left(\frac{L}{v}\right)_L^m \frac{k_f}{L} A(T_\infty - T_{1o})}{\rho c_p V s + cV_o^m\left(\frac{L}{v}\right)_L^m \frac{k_f}{L} A} \times \frac{V_\infty}{62} \times \frac{(0.09)}{s} \quad (34)$$

Finally,

$$\frac{\Delta P(s)}{\Delta error(s)} = K(s) \quad \text{Controller} \quad (35)$$

By expanding and simplifying , the open loop system in its final form is

$$\frac{\Delta T_1(s)}{\Delta error(s)} = \frac{(0.09)V_\infty cmV_o^{m-1}\left(\frac{L}{v}\right)_L^m \frac{k_f}{L} A(T_{1o} - T_\infty)}{s \cdot \left(s + \left(\frac{cV_o^m\left(\frac{L}{v}\right)_L^m \frac{k_f}{L} A}{\rho c_p V} \right) \right)} \times K(s) \quad (36)$$

The final form of the open loop transfer function shown in Equation (36) indicates that the system is a second order system with a pole at the origin and a pole in the left half plane. Two other observations can be made from this transfer function. First, the freestream airspeed V_∞ and the difference between the nominal point temperature T_{1o} and freestream temperature T_∞ act much like a proportional gain. Second, the thermal capacitance will influence the speed of the response. A large thermal capacitance will slow down the system response. To evaluate a specific operating condition where surface temperature is steady at 35 deg C, ambient temperature is steady at 19 deg C, and

freestream airspeed is at 8.9 m/s, the constants and nominal point values substituted into Equation (36) are:

$$\begin{aligned} c &= 0.2125, \quad m = 0.675, \quad V_o = 6.087 \text{ m/s}, \\ L &= 0.0222 \text{ m}, \quad v = 0.000016 \text{ m}^2/\text{s}, \quad k_f = 0.026 \text{ W/mK}, \\ T_\infty &= 292 \text{ K}, \quad T_{lo} = 308 \text{ K}, \quad A = 0.0016 \text{ m}^2, \quad \rho c_p V = 5.86 \text{ J/K} \end{aligned}$$

After the substitution, the open loop transfer function (Equation (36)) reduces to

$$\frac{\Delta T_1(s)}{\Delta error(s)} = \frac{0.000696}{s(s + 0.0304)} \times K(s) \quad (37)$$

A PD controller was used, which has the form

$$K(s) = K_p + K_d s = K_d \left(s + \frac{K_p}{K_d} \right) \quad (38)$$

By placing the zero at $s = -0.1$ such that the controller $K(s) = K_d (s + 0.1)$, the system response speeds up with increasing values of K_d . MATLAB's[®] RLOCUS command generated the root locus diagram shown in Figure 32.

The performance of the PD controller was compared against the scheduled proportional controller from the previous section at the same three freestream airspeed and temperature difference conditions (Conditions 1, 3 and 8 in Table 5). The PD controller was designed to match the scheduled proportional gain controllers temperature overshoot for Condition 1. The values of this controller were $K_p = 6.0$ and $K_d = 60$.

The PD controller design proved to be superior to the scheduled proportional controller design (this controller was not tested experimentally). Figure 33 shows a comparison of the simulation responses when the PD and scheduled proportional controllers were used at Condition 1 in Table 5. The PD controller significantly reduces

the number of oscillations in the temperature and inlet responses. Using the same values for the PD controller, the response comparison for Condition 3 is shown in Figure 34. Again, the PD design is superior to the controller in Figure 30. It shows better temperature regulation (6 % temperature overshoot instead of 10 %) and significantly reduced inlet control usage. The outstanding PD performance continues at Condition 8 shown in Figure 35. Again, the PD design shows better temperature regulation (7 % temperature overshoot instead of 9 %) and reduced inlet control usage.

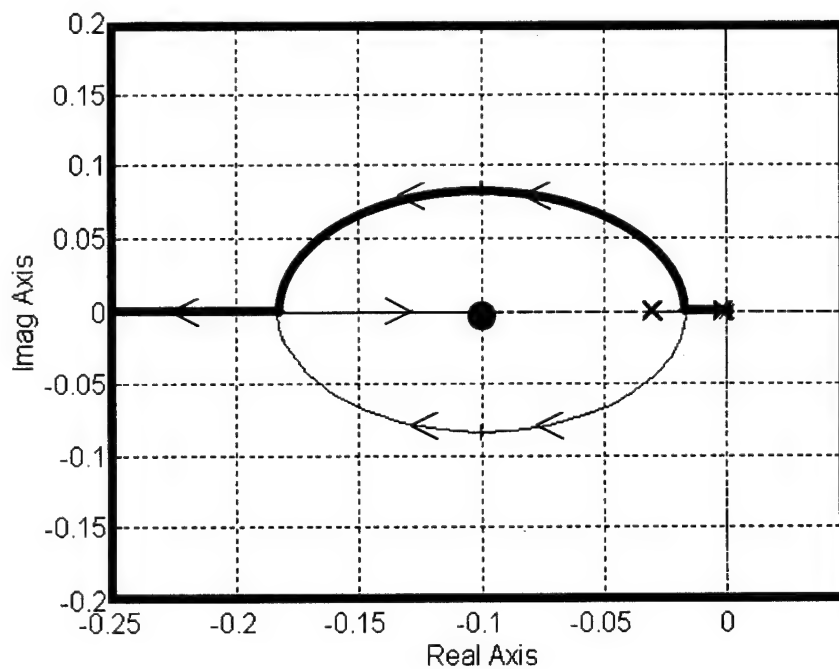
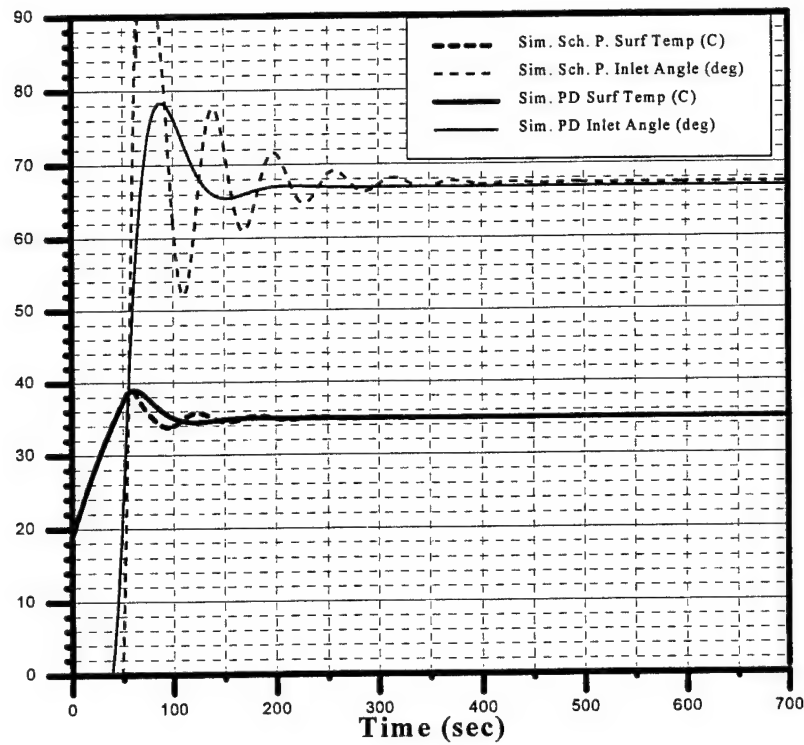


Figure 32. Root Locus Diagram with a zero at $s = -0.1$

There are a few significant observations that can be drawn from this evaluation. First of all, the linearized transfer function detailed in Equation (36) requires a lot of information about the nominal point being evaluated. Unless a prototype system is available, this data may not be available and will need to be estimated. Second, a PD

controller with performance characteristics similar to those shown in this section can be found for any hardware systems that can be modeled in the form of Equations (24), (31), and (33). Lastly, a PD controller designed with one thermocouple outperforms a scheduled proportional controller design that utilized two thermocouples and an airspeed sensor.



**Figure 33. Comparison of Scheduled Gain (P) and PD Controllers
Condition 1, Ref Temp-35(C), Freestream Airspeed-8.9(m/s)**

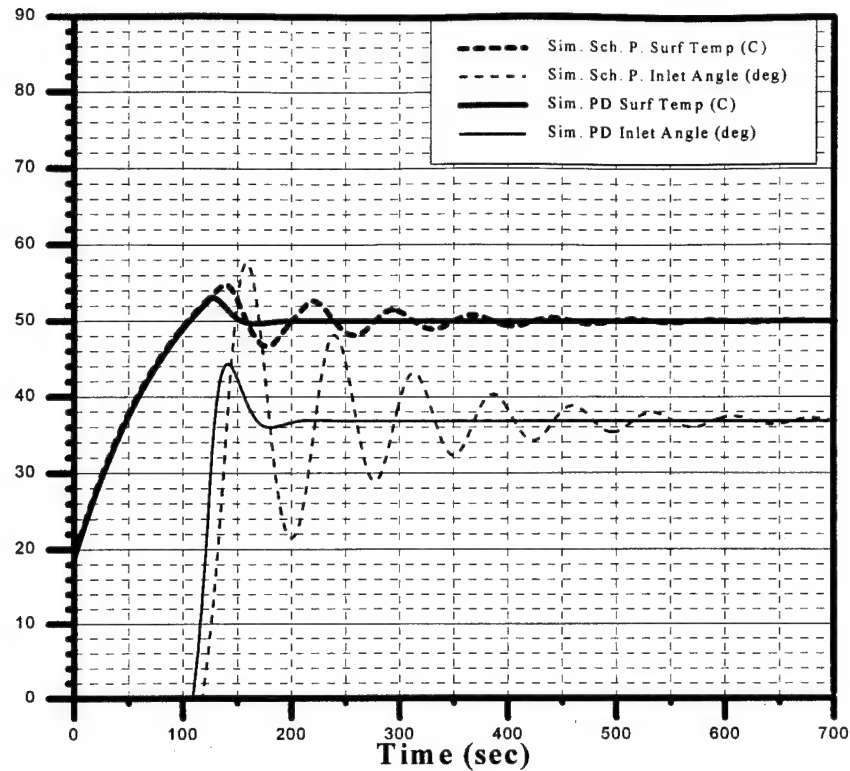


**Figure 34. Comparison of Scheduled Gain (P) and PD Controllers
Condition 3, Ref Temp-50(C), Freestream Airspeed-8.9(m/s)**

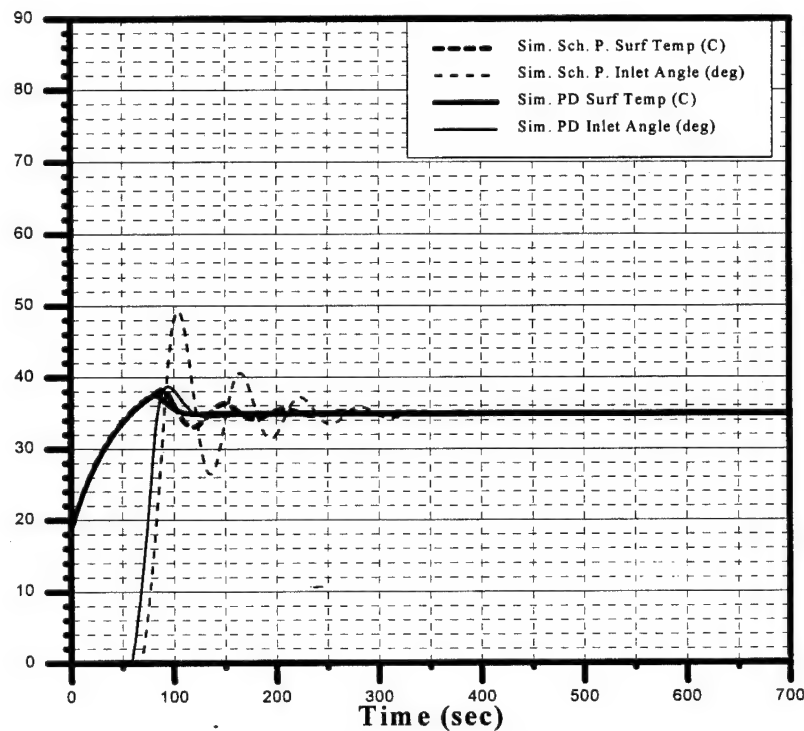


**Figure 35. Comparison of Scheduled Gain (P) and PD Controllers
Condition 8, Ref Temp-35(C), Freestream Airspeed-26.8(m/s)**

MATLAB[®] Nonlinear Toolbox Controller Design

The final method that was used to design a controller required a well-correlated SIMULINK[™] model. With this model and the Nonlinear Control Design (NCD) Toolbox, a proportional-integral-derivative (PID) controller was designed. For background purposes, the NCD Toolbox automatically converts time domain constraints into a constrained optimization problem that is solved with routines from the MATLAB[®] Optimization Toolbox. The plant can be nonlinear. In the solution process, the NCD Toolbox iteratively compares the SIMULINK[™] simulation responses with the constraint objectives and the tunable parameters are then adjusted with gradient methods. [11]

The design process is initiated by connecting the NCD icon to the SIMULINK[™] simulation response that needs to be adjusted. With the icon connected, the response boundaries (constraint window) and controller variables are defined by the user. Figure 36 shows the unacceptable region as black. In this study, the controller was assumed to be of the form

$$K(s) = K_p + \frac{K_i}{s} + K_d s = \frac{K_d \left(s^2 + \frac{K_p}{K_d} s + \frac{K_i}{K_d} \right)}{s} \quad (39)$$

so that the variables are K_p , K_i , and K_d . Lastly, since the values of K_p , K_i , and K_d are adjusted with gradient methods, the simulation needs initial values for K_p , K_i , and K_d .

The need for initial values gives rise to a limitation. If poor initial values are used, the algorithm may not be able to obtain the desired performance response. For example, the NCD program failed when the constraint window shown in Figure 36 was used to design a PID controller with initial values of $K_p = 8$, $K_i = 0$, and $K_d = 0$. Consequently,

the designer needs a good idea of the values that will be used for each of the controller variables. When the previous PD controller values ($K_p = 6$, $K_i = 0$, and $K_d = 60$) were used as initial conditions with the constraint window shown in Figure 36, the algorithm converged to the values of $K_p = 4.72$, $K_i = -0.00072$, and $K_d = 100.0$. This corresponds to a controller of the form

$$K(s) = \frac{100(s^2 + 0.0472s - 0.0000072)}{s} = \frac{100(s + 0.047)(s - 0.000152)}{s} \quad (40)$$

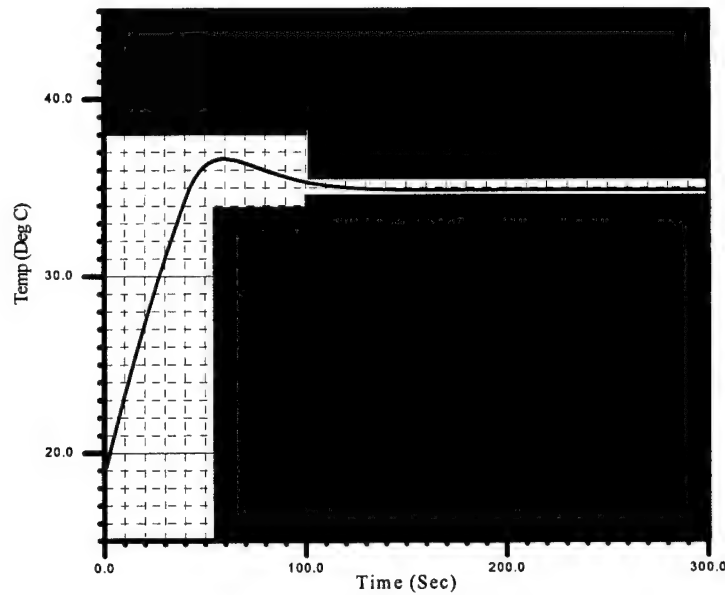


Figure 36. NCD Design Constraint Window with PID Controller Response

The response shown in Figure 36 and the root locus diagram in Figure 37 correspond to the controller in Equation (40). Figure 37 is similar to the PD root locus in Figure 32 with the addition of a pole at the origin, a new zero at 0.000152, and the zero moved in to $s = -0.047$ from the $s = -0.1$ location.

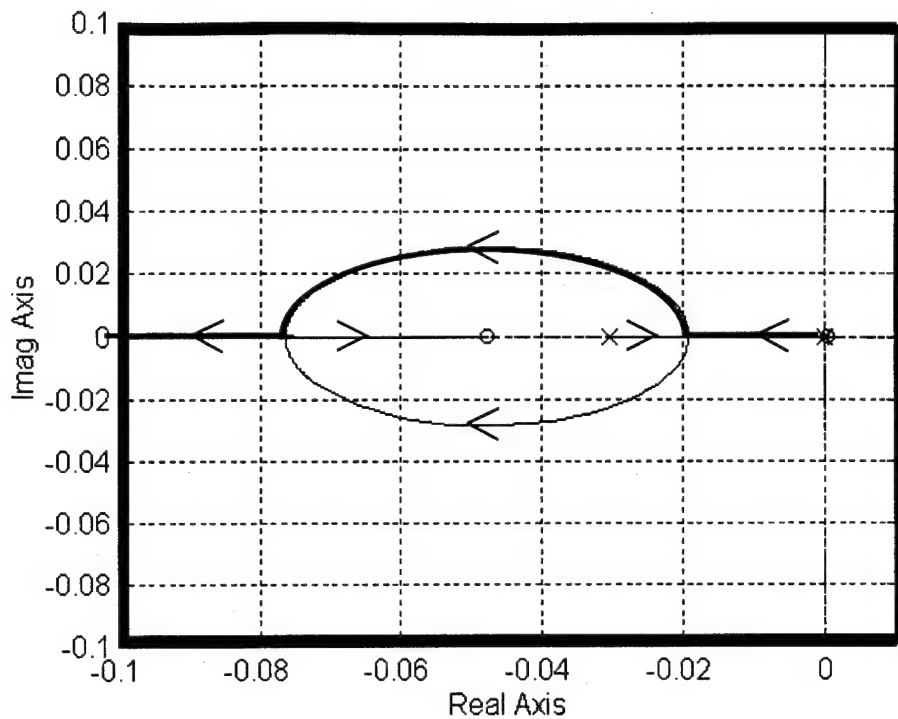


Figure 37. Root Locus Diagram of NCD PID Controller

This PID controller was compared against the previous PD controller design (this PID controller was not tested experimentally). In addition, it should be noted that this comparison may be considered unfair. The NCD designed controller was optimized on the nonlinear model. The root locus designed controller used the linearized model and it was not optimized. However, Figures 38 through 40 show the comparison of the two controllers at the previous three conditions (Conditions 1, 3 and 8 in Table 5). The PID controller performs better than the PD controller at all three conditions. The temperature overshoots are almost eliminated and there appears to be no need for any gain scheduling.

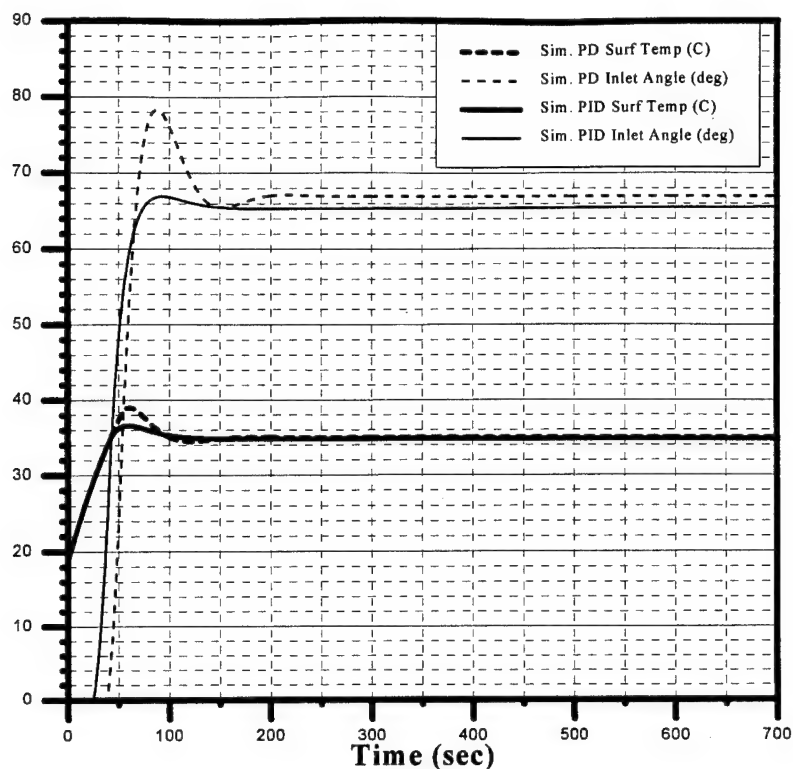


Figure 38. Comparison of PD and PID Controllers
Condition 1, Ref Temp-35(C), Freestream Airspeed-8.9(m/s)

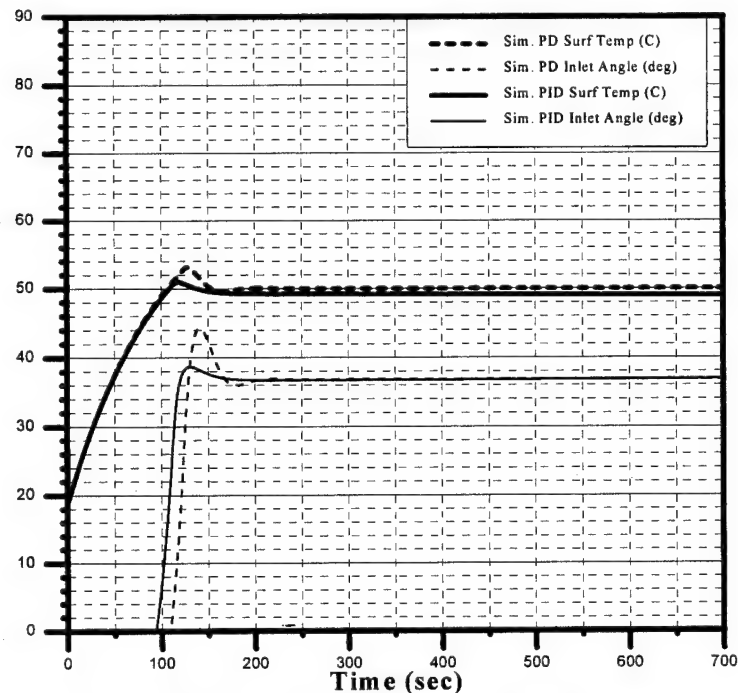
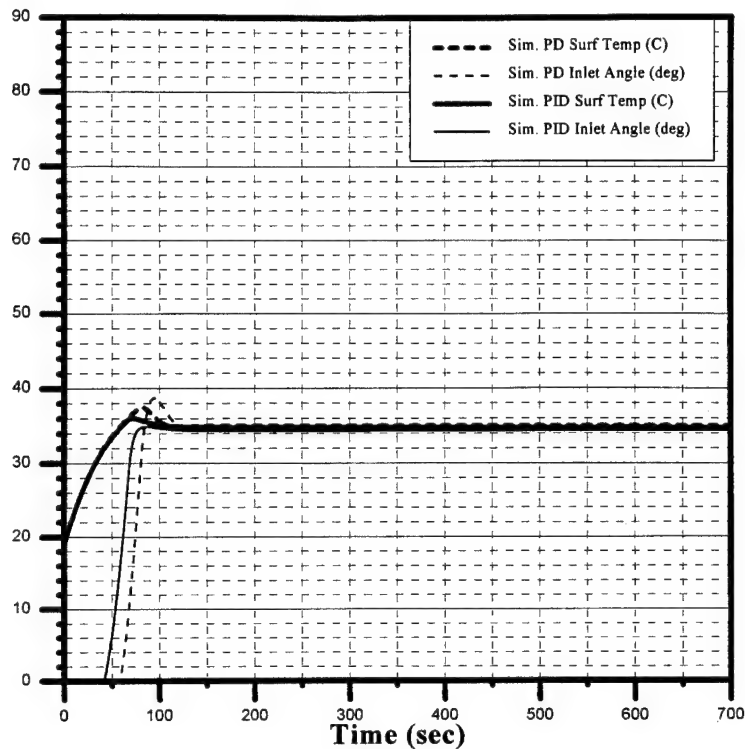


Figure 39. Comparison of PD and PID Controllers
Condition 3, Ref Temp-50(C), Freestream Airspeed-8.9(m/s)



**Figure 40. Comparison of PD and PID Controllers
Condition 8, Ref Temp-35(C), Freestream Airspeed-26.8(m/s)**

Noise, Changing Reference Temperature, and Experimental PID Data

The PD and PID controllers have shown themselves to be well performing controllers in the simulation model for a standard input. To check the system response to different inputs, the reference temperature was modified. The modified command input set reference temperatures to 35 deg C for the first 300 seconds, 40 deg C for 301-600 seconds, and back to 35 deg C for the last 601-1000 seconds. In addition, white noise was also added to the thermocouple signal. Figure 41 shows an actual sample of the noise that was added to the simulation surface temperature signal.

The responses of the PD and PID controllers with the new command input and the added noise are shown in Figure 42. The PID controller regulates temperatures

slightly better than the PD controller (temp. overshoot of 4% compared to 11%), but shows no improvement with respect to noise. Also, both inlet responses show spikes at 300 & 600 seconds, which the hardware could not achieve.

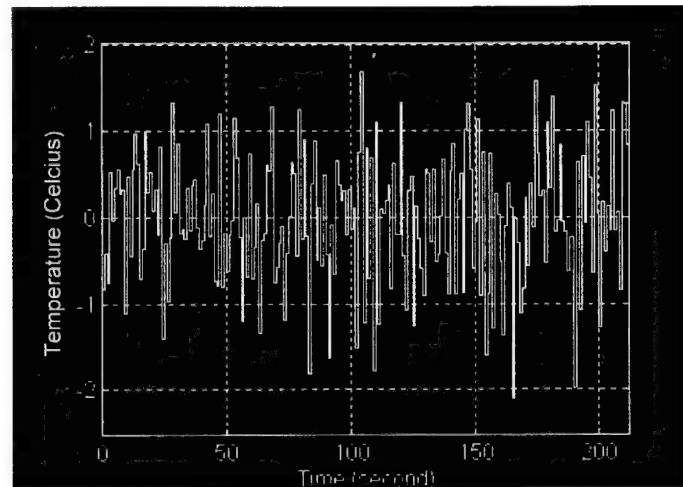
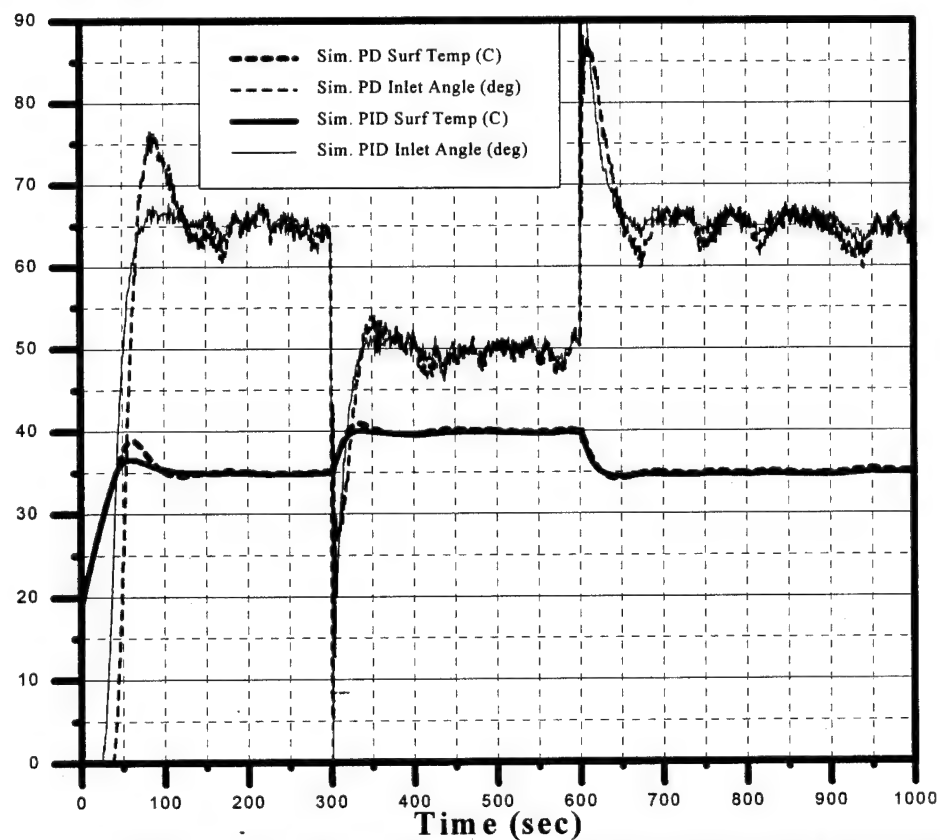


Figure 41. Actual Sample of White Noise Added to Simulation Temperature Signal



**Figure 42. PD & PID Controllers with Noise and Modified Control Schedule
Freestream Airspeed- 8.9(m/s)**

To check the accuracy of the simulation model with the actual hardware for more complex controllers, a PID controller was tested on the simulation and experimentally. It would have been desirable to test the PID controller defined in Equation (40), but it was not designed at the time of testing. Fortunately, a similar PID controller was designed at that time. The PID controller that was tested experimentally (referred to as PID_{lab}) was obtained with the NCD toolbox, but it was derived with a different constraint window and different initial conditions. The values of the PID_{lab} variables were $K_p = 2.92$, $K_i = -0.0015$, and $K_d = 45.0$. This corresponds to a controller of the form

$$K(s) = \frac{45(s^2 + 0.0649s - 0.000033)}{s} = \frac{45(s + 0.065)(s - 0.0005)}{s} \quad (41)$$

The root locus for the system with the controller in Equation (41) is similar to the root locus in Figure 37 with the zeros moved from - 0.047 to - 0.065 and from 0.000152 to 0.0005.

The results shown in Figure 43 indicate that the temperature responses are very similar, the responses due to noise are similar, and the simulation had a slight inlet correlation error (as noted earlier for Figure 27). Figure 43 also indicates that the simulation inlet reacts and moves faster than the actual hardware inlet. The inlet spikes are not seen at 300 & 600 seconds in the experimental data.

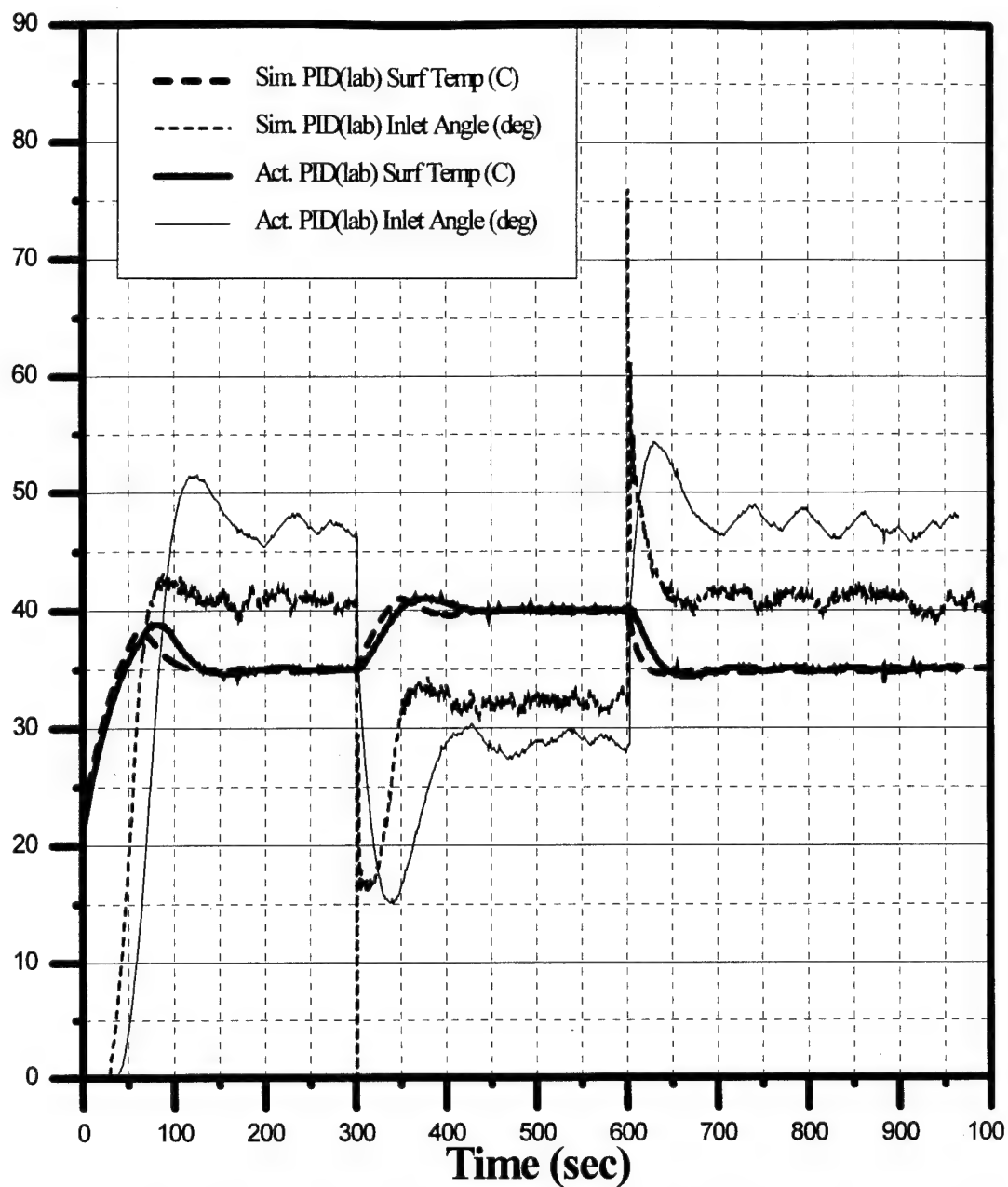


Figure 43. Comparison of Simulation and Hardware Responses to similar PID(lab) Controllers. Freestream Airspeed- 26.8(m/s)

V. APPLICATION

Controller Design Approach

After developing the prototype hardware and software models, a design approach for implementing a variable area inlet was synthesized. This design process will provide thermal control designers with a structured design approach. The process consists of ten steps and it was modeled after the general design process detailed in Franklin et al. [3]. Keep in mind that this approach may not be the only approach for every application and as a result, engineering judgment should be exercised throughout the whole process.

STEP 1. Understand and define the thermal performance requirements. In the problem definition clearly identify the exact location of the component that requires temperature regulation. At this location identify temperature and performance constraints like maximum allowable temperature, desired operating temperature, temperature cycle limitations, and time response limits to a step input.

STEP 2. Understand and define the operating environment. Remember that the purpose of the variable area inlet is to change the inlet area to minimize drag in a changing vehicle environment. The design points should consider the extreme and nominal conditions of each changing variable in the vehicles environment. In this study, the changing variables were freestream temperature and freestream airspeed. In other applications additional variables may change also. One such variable might be the freestream fluid properties.

STEP 3. Select a sensor. With the exact location and operating environment known, choose a sensor that can accurately measure the temperature of the exact location while being able to survive and perform well in the operating environment.

At this point, trade studies may be required. For example, due to geometry or environmental constraints, it might be impossible to place a sensor at the exact location that is to be temperature regulated. As a result, a thermal analysis may be required to find the next best place to locate the sensor.

STEP 4. Design the variable geometry inlet. In general, this is a very application-specific step and each design will have unique constraints. However, every design will need to consider the worst case operating environment, airflow characteristics, and actuating torque requirements. First of all, every inlet design must be capable of providing sufficient airflow while in a wide open position while operating in a worst case environment. Therefore, this is an excellent criteria to start the inlet design process.

Second, attention should be given to the flow characteristics of the inlet. Try to choose an inlet that will provide changes to the cooling air airspeed over the entire range of inlet positions. For example, in this study it was found that the inlet had a small effect on the test section airspeed for the first 28 degrees of inlet travel. This dead zone reduced the temperature control performance because it took extra time to travel through this range before increased cooling airspeed was observed. Lastly, when designing the inlet try to minimize the actuating torque requirements. This will help to reduce the actuator size, weight, and power requirements.

STEP 5. Select an actuator. Similar to the inlet design, the actuator selection is application specific. Some aspects to consider include torque requirements, open/close rates, weight, and cost.

STEP 6. Estimate or empirically determine the Nusselt number. With the shape of the component and the anticipated cooling airflow pattern, estimate a Nusselt number or perform testing to empirically determine a Nusselt number.

STEP 7. Simulate. With the inlet, actuator, and Nusselt number known, simulate the temperature response to various operating conditions. If the components have been acquired, perform component level testing to understand their performance characteristics. Try to model these characteristics to increase the accuracy of the simulation. If the system can be assembled, perform preliminary system tests with a simple proportional controller. Make necessary adjustments to improve the simulation's match to the actual data.

STEP 8. Try a PD controller. With data from the working simulation, obtain numerical values for the nominal point variables that the controller will be designed about. Put these numerical values into the linearized model of the system. Place the zero of the PD controller two to five times farther out in the left half plane than the largest negative pole value. Increase the controller gain and shift the location of the zero until a satisfactory response is obtained. If the system has been assembled, try a test run with the PD controller to see if the models compare favorably with the PD controller.

STEP 9. Optimize with a PID controller. With a well performing PD controller, use MatLab's NCD Toolbox to optimize a PID controller.

STEP 10. Test. Test the final system in its actual operating environment.

VI. CONCLUSIONS

1. A working hardware model of a variable area inlet was built and tested. The hardware model validated the concept that a variable area inlet could regulate a component temperature with ram air.
2. A simulation model of the physical system was constructed and the simulation responses compared favorably with the hardware model responses. As a result of the favorable comparison, the simulation model demonstrated that it did not require a linearized thermal plant. The simulation also modeled the convection coefficient as a variable with velocity as an input to the thermal plant. Future applications could modify the simulation in this thesis to help in the design process.
3. A scheduled proportional gain controller can be designed for a varying freestream temperature and airspeed environment with least squares methods. This controller will require increased system complexity by requiring a freestream temperature sensor and a freestream airspeed sensor. The scheduled proportional gain controller performs better than a fixed gain proportional controller by regulating temperature better while using less control in a varying environment.
4. The linearized system reveals that the denominator of the open loop system used in this thesis has a root at the origin and another negative root. This linearized thermal plant uses velocity as the input and has temperature as the output. The linearized thermal plant can be used in future control designs. By using a root locus diagram and designing a PD controller with a zero that has a magnitude larger than the largest denominator root, an

improvement to the dynamic proportional controller can be realized. The major improvement is the reduction in control oscillations. Furthermore, unlike the proportional controller, the PD controller does not appear to require any gain scheduling for the range of freestream airspeeds and temperature differences that were used in this thesis. This eliminates the need for additional sensors.

5. A PID controller designed with the nonlinear control design toolbox performs better than the PD controller by nearly eliminating the temperature overshoot. Like the PD controller, the PID controller does not appear to require any gain scheduling for the range of freestream airspeeds and temperature differences that were used in this thesis.

6. A general design process was constructed. Specific lessons that were learned from this study will benefit future applications. The lessons include; eliminating dead zones in the inlet flow characteristics, reducing inlet torque requirements, and designing a controller that reduces temperature overshoots and inlet control oscillations.

7. The results from Lofkin [1] and Carr [2] indicate that a significant portion of the drag coefficient on vehicles results from internal cooling airflow. These vehicles use ram air to cool internal combustion engines.

VII. RECOMMENDATIONS

1. This study maintained the component at low temperature to minimize radiation losses. Additional studies could be performed on a high temperature component to add in the effects of radiation to the thermal control model and the simulation model.
2. This study proved that the freestream air properties remained relatively constant with respect to freestream air temperature variations. Additional studies could be performed to evaluate the controller changes that would be required for air property variations with altitude.
3. This study evaluated the system at low freestream airspeeds. Additional studies could evaluate the system at high freestream airspeeds.
4. The flow characteristics of the inlet could be retested to see if better data could eliminate the leakage correlation step.
5. The thermal model could include a conduction term to see if it would eliminate the need for a correlation step to correct the heat generation and thermal capacity values.
6. The linearized system could be optimized with the nonlinear control design toolbox to compare the optimal performance on the nonlinear and linear systems.

REFERENCES

1. Lofkin, Laurence K. Subsonic Aircraft: Evolution and the Matching of Size to Performance, NASA Reference Publication 1060, August 1980
2. Carr, G. The Influence of Engine-Cooling Airflow on Car Performance and Stability, Institution of Mechanical Engineers, 1995, C496/079/95
3. Franklin et al. Feedback Control of Dynamic Systems Third Edition, Addison-Wesley Publishing Company, Inc., 1994
4. Close, Charles M. and Dean K. Fredrick. Modeling & Analysis of Dynamic Systems Second Edition, Houghton Mifflin Corp., 1993
5. Cannon, Robert H. Jr. Dynamics of Physical Systems, McGraw-Hill, Inc., 1967
6. Incropera, Frank P. and David P. DeWitt. Fundamentals of Heat and Mass Transfer Third Edition, John Wiley & Sons, 1990
7. Lindeburg, Michael R. Mechanical Engineer Reference Manual Eighth Edition, Professional Publications, INC., 1990, pp.6-2,6-27
8. Roots, William K. Fundamentals of Temperature Control, Academic Press, Inc., 1969
9. Grace, Andrew, and Joseph Hicklin. SIMULINK™ User's Guide, The MathWorks, Inc., 1992
10. Tal, Jacob. Step-By-Step Design of Motion Control Systems, Galil Motion Control, Inc., 1994
11. Potvin, Andrew F. Nonlinear Control Design Toolbox, The MathWorks, Inc., 1993

APPENDIX A. AIR PROPERTIES ANALYSIS

A computer program was developed to interpolate tabulated air properties as a function of temperature. The properties were obtained from Incropera & DeWitt [5]. The air properties were then used to calculate the convection coefficient from the Nusselt number. The conditions for the calculations were: airspeed = 17.9 m/s, surface temperature = 40.0 deg C, length = 0.0222 m. The three Nusselt numbers and their corresponding percent change in convection coefficient over the temperature range from 250 K to 400 K were:

- | | | |
|-----------------------------------|--|---------------|
| a. Flat Plate in Laminar Flow - | $0.332 \text{ Re}_x^{1/2} \text{ Pr}^{1/3}$ | 0.09 % Change |
| b. Flat Plate in Turbulent Flow - | $0.0296 \text{ Re}_x^{4/5} \text{ Pr}^{1/3}$ | 12.6 % Change |
| c. Empirical Thesis Nusselt No. - | $0.25 \text{ Re}_x^{.65}$ | 6.36 % Change |

Computer Code

```
% This program takes the Nusselt number for a Flat Plate in
% Laminar & Turbulent flow and the electric component and evaluates
% the variation in the convection coefficient (h) when the temperature
% changes between 250-400 Kelvin

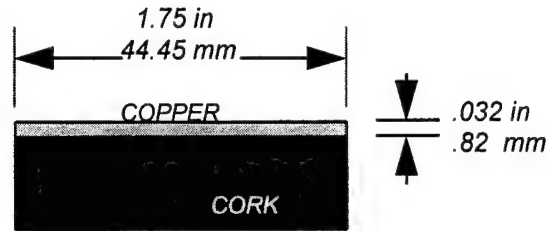
% Air Properties from Incropera & Dewitt - Dry air 1-ATM
prop1(:,1)=[250,300,350,400]';
prop1(:,2)=10^(-6)*[11.44,15.89,20.92,26.41]';
prop1(:,3)=[.72,.707,.700,.69]';
prop1(:,4)=10^(-3)*[22.3,26.3,30,33.8]';

% Input Data (Temp-Kelvin, Velocity-MPH) and Calculate hx
Velo1=(.447)*[40];
Ts1=40+273;

%Calculate hx - Flat plate & Empirical Equations
for j=1:16;
    Tamb1(j)=(240+(10*j));
    Tfilm1(j)=((Ts1+Tamb1(j))/2);
    prop1=table1(prop1,Tfilm1(j));
    hxtl(j)=.332*(Velo1*.0222/prop1(1))^(.5)*(prop1(2)^(1/3))*prop1(3)/.0222;
    hxtt(j)=.0296*((Velo1*.0222/prop1(1))^(4/5))*(prop1(2)^(1/3))*prop1(3)/.0222;
    %hthew(j)=.25*((Velo1*.0222/prop1(1))^(.65))*(prop1(2)^(1/3))*prop1(3)/.0222;
    hthewo(j)=.25*((Velo1*.0222/prop1(1))^(.65))*prop1(3)/.0222;
end

%Plot Heat Transfer Coefficient vs Velocity
plot(Tamb1,hxtl,'-',Tamb1,hxtt,'-',Tamb1,hthewo,'-'),...
title('Local Heat Transfer Coefficient vs Temperature'),...
ylabel('Local Heat Transfer Coefficient (watt/meter^2*K)'),...
xlabel('Temperature (K)')
legend('Laminar','Turbulent','Thesis w/o Pr')
axis([250,400,0,250])
```

APPENDIX B. CONDUCTION ANALYSIS



Copper Surface (A_1) = 0.0016 square meters (top + sides)

L = 0.0127 meters (cork thickness)

Properties (Incropera & DeWitt)

k_{cork} = 0.039 (w/K*m²)

emissivity (ϵ) copper = 0.2 (estimated)

Conductive Losses

Conductive losses were calculated by assuming the copper was isothermal and the cork was a pin fin with an exposed end. The energy equation was written for steady state conditions. With the isothermal copper temperature and ambient temperature known, the value of the convection coefficient was iterated on until the heat generation rate matched the actual measured value of 3.39 watts (see Matlab Program). When the equation was balanced, the percentage heat loss due to all three modes of heat transfer was calculated.

The energy balance was written as

$$\frac{kA}{L}(T_1 - T_\infty) + \sigma A \epsilon (T_1^4 - T_\infty^4) + hA(T_1 - T_\infty) = q_{gen}$$

where the conduction term is replaced by the fin heat transfer equation [5]

$$\frac{kA}{L}(T_1 - T_\infty) = M \frac{\sinh mL + (h/mk) \cosh mL}{\cosh mL + (h/mk) \sinh mL}$$

$$M = \sqrt{hPkA} \cdot (T_1 - T_\infty)$$

$$m = \sqrt{hp/kA}$$

Velocity (m/s)	Surf Temp (C)	% Rad Loss	% Cond Loss	% Conv Loss
2.2	67.2	3	22	75
4.1	49.8	2	18	80
8.6	40.3	1	15	84
13.1	36.6	1	13	86
17.7	34.3	1	12	87
22.2	32.9	0.5	11.5	88
26.8	31.9	0.5	11	88.5

Computer Code

```
% This program takes the thermal parameters of the system and
% returns a heat loss percentage from convection, conduction,
% and radiation. Conduction is based on a pin fin exposed tip
% equation from Incropera & Dewitt.

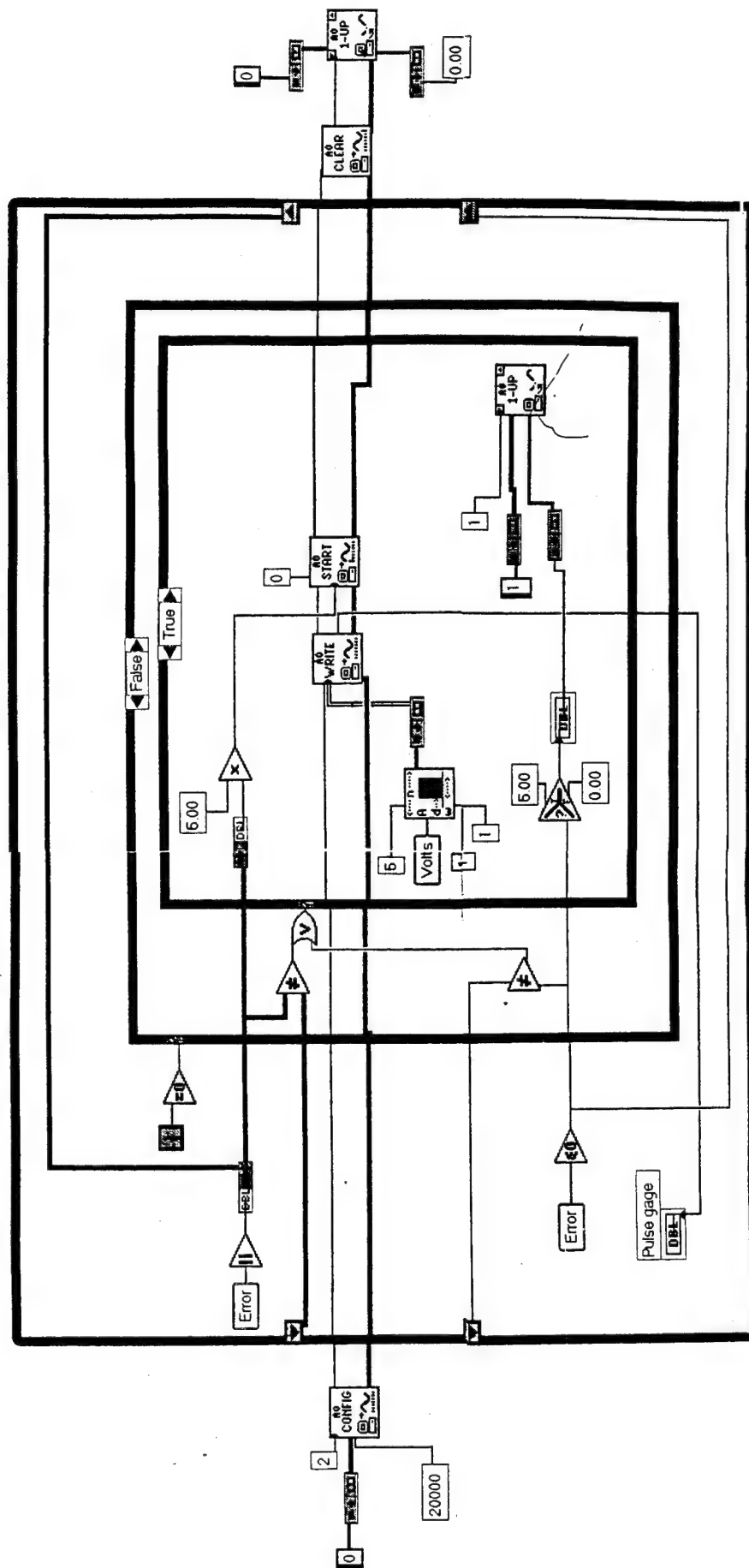
% Define system parameters
T1=305.15;
h=228.3;
Ta=296.9;
SACOP=0.0016;
P=(pi*(0.04445));
Ac=((pi/4)*((0.04445)^2));
k=0.039;
e=0.2;
Sigma=(5.67*10^(-8));
L=0.0127;
M=((h*P*k*Ac)^.5)*(T1-Ta));
m=((h*P)/(k*Ac))^.5);

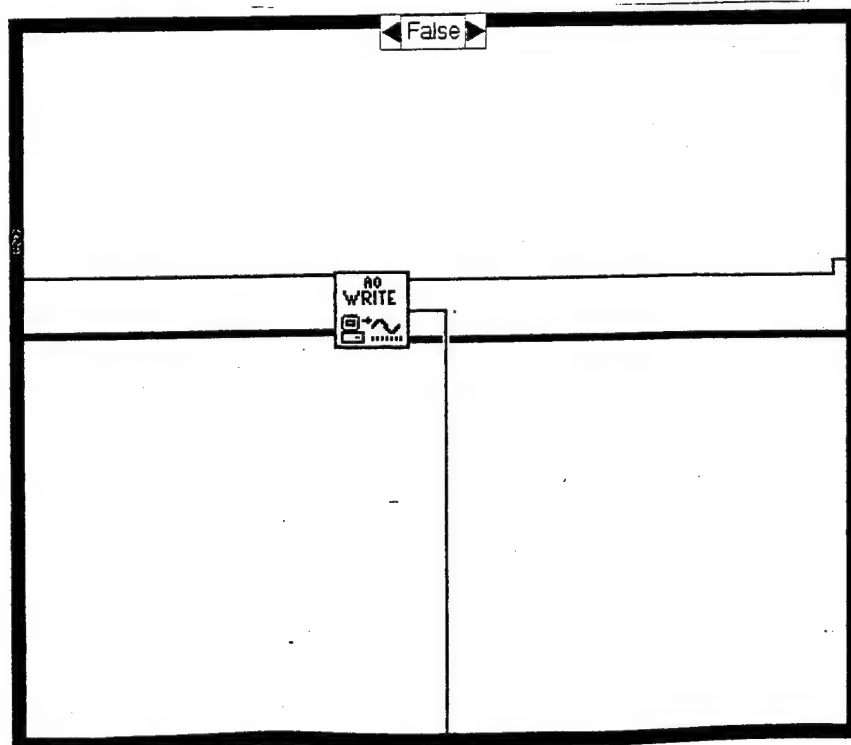
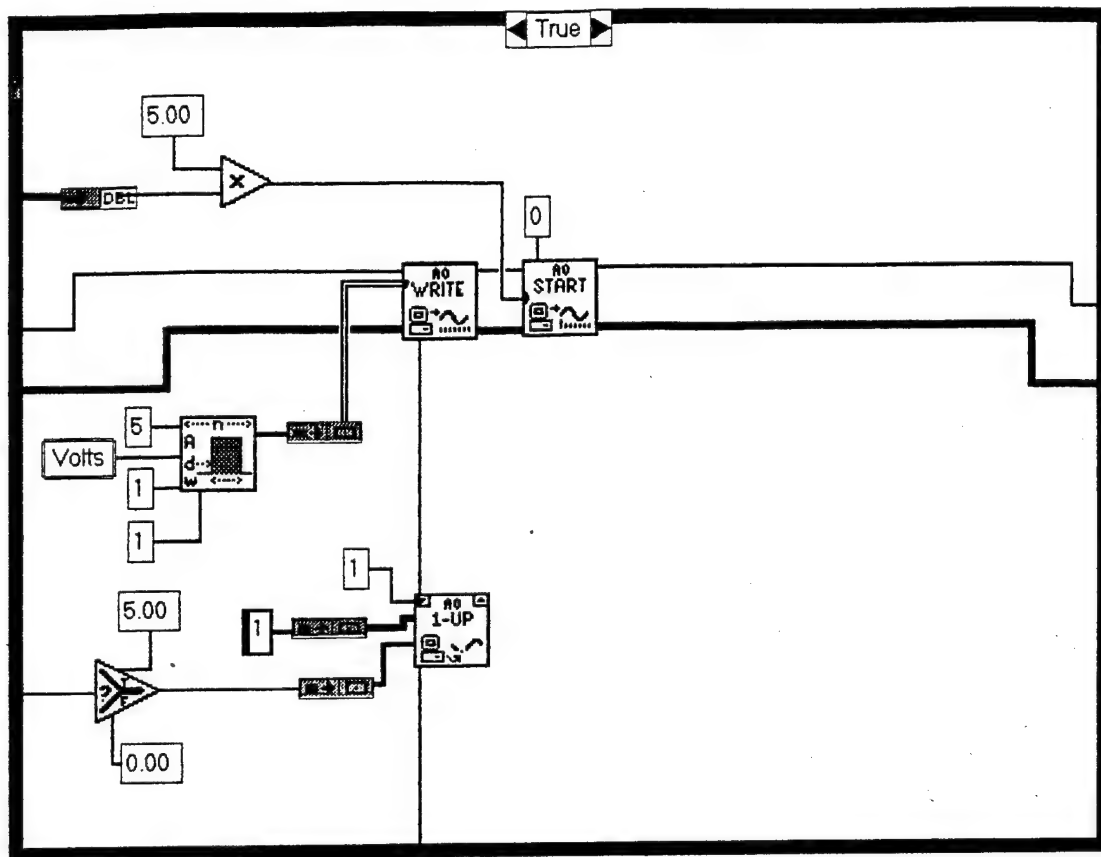
% Energy Equation
q=(h*SACOP*(T1-Ta))+(Sigma*SACOP*e*(T1^4-
Ta^4))+(M*((sinh(m*L))+((h/(m*k))*(cosh(m*L))))/((cosh(m*L))+
((h/(m*k))*(sinh(m*L)))))

% Calculate % Losses
Pctqconv=(h*SACOP*(T1-Ta))/q
Pctqgrad=(Sigma*SACOP*e*(T1^4-Ta^4))/q
Pctqcond=(M*((sinh(m*L))+((h/(m*k))*(cosh(m*L))))/((cosh(m*L))+
((h/(m*k))*(sinh(m*L)))))
```

APPENDIX C. LabView™ Subroutine

The following diagrams are included to document the programs that were written to perform the data acquisition and temperature control tasks. The following pages will not include a narration of the logic.





APPENDIX D. INLET DYNAMICS TEST

Objective

The objective of this experiment was to determine the test section airspeed relative to the freestream airspeed and inlet angle.

Approach

The freestream airspeed was held constant and a pitot tube positioned in the test section near the electric component location. With a constant freestream airspeed, the inlet angle was adjusted from 0-90 degrees in 9 degree increments. At each increment, the pitot tube values were recorded. When the inlet made the full 0-90 degree rotation, the freestream airspeed was increased and the process was repeated.

Equipment

- 2 - Pitot Static Probes
- 2 - Differential Pressure Transducers
- 1 - Water Manometer
- 1 - AeroLab Tech Low Speed Wind Tunnel
- 1 - LabView Computer Board & Associated Software

Set-Up

1. The duct and inlet assembly were mounted on the bottom-center of the wind tunnel test section in a parallel orientation.
2. Airspeed Measurement - Pitot static probes were placed in the freestream air and at a location near the component mounting location in the test section. The total and static lines were routed in parallel to water manometer and differential pressure transducers.

The differential transducers and wind tunnel velocity recording instruments were zeroed. The manometer reading was sufficient for the larger airspeeds. However, at the low end of the airspeeds, the manometer accuracy was reduced and greater resolution was obtained from the tunnel and transducer readings. Nevertheless, the average of these four readings was used.

Procedure

1. All instruments were turned on and were allowed to warm up for at least 30 minutes before being zeroed. Ambient conditions were recorded:

RUN1: 12 May 95 , 1700hrs

T ambient = 23.0 C

Pressure = 28.932 in Hg

%Rel Hum= 43%

2. Freestream airspeeds were set at 26.8, 22.4, 17.9, 13.4, 8.9, 4.5, and approx. 2-3 m/s.

Inlet angles were increased from 0-90 degrees in 9 degree increments. Pitot data was recorded at each increment.

APPENDIX E. COMPONENT ORIENTATION TEST

Objective

The objective of this test was to determine the best orientation of the component relative to the freestream airspeed to maximize convective heat losses.

Approach

A thin resistance heater was applied to a thin copper disc. Heat generation was held constant by maintaining a constant voltage and current. The freestream airspeed was held constant and the component was rotated in 30 degree increments. After rotating the component from 0-180 degrees, the freestream airspeed was increased and the rotation process was repeated. At each airspeed and position, the surface temperature was recorded.

Equipment

- 3 - "T" Type thermocouples
- 3 - Omega Ice Points
- 3 - Thermocouple Amplifiers with Low-Pass Filters (Measurements Group model 2310)
- 2 - Pitot Static Probes
- 2 - Differential Pressure Transducers
- 1 - Water Manometer
- 1 - 114 Ohm Thin Film Electrical Heater (Minco)
- 1 - Power Supply (Sorensen DCR-13B)
- 2 - Digital Multimeters (HP 34401A)
- 1 - AeroLab Tech Low Speed Wind Tunnel
- 1 - LabView Computer Board & Associated Software

Set-Up

1. The component was mounted in the center of the wind tunnel test section. A position indicator was used to adjust the orientation in 30 degree increments.
2. Airspeed Measurement - Pitot static probes were placed upstream and below the component. The total and static lines were routed in parallel to water manometer and differential pressure transducers. The differential transducers and wind tunnel velocity recording instruments were zeroed. The manometer reading was sufficient for the larger airspeeds. However, at the low end of the velocities, the manometer accuracy was reduced and greater resolution was obtained from the tunnel and transducer readings. Nevertheless, the average of these four readings was used.
3. Temperature Measurement - Extra care was placed in mounting the thermocouples. For measuring surface temperature, a small dimple was placed in the center of the copper. The thermocouple end was placed inside the dimple and a punch was used to form the copper around the junction creating a mechanical joint. The wires were then carefully covered with electrical tape so that they did not act as pin fins. All wires were routed directly back in effort to keep the airflow undisturbed in front of the thermocouples. All thermocouples were zeroed to an Omega Thermocouple Calibrating Instrument.

Procedure

1. All instruments were turned on and were allowed to warm up for at least 30 minutes before being zeroed. Ambient conditions were recorded:

RUN1: 21 April 95 , 0600hrs

T ambient = 22.75 C

Pressure = 28.670 in Hg

%Rel Hum= 57%

2. Power supply was turned on and the component was allowed to stabilize in a natural convection environment (approx. 20 minutes)
3. Wind tunnel velocities were increased to 26.8 m/s and held until no temperature changes were observed on the component for a 200 second interval. The velocity and surface temperature readings were recorded. Data was recorded at freestream airspeeds 26.8, 22.4, 17.9, 13.4, 8.9, 4.5, and approx. 2-3 m/s.

APPENDIX F. CONVECTION COEFFICIENT TEST

Objective

The objective of this experiment was to determine the Nusselt number for the heat generating component.

Approach

A thin resistance heater was applied to a thin copper disc. Heat generation was held constant by maintaining a constant voltage and current. The freestream airspeed was adjusted and the surface temperature was recorded. With heat flux, surface temperature, and ambient temperature known, the local convection heat transfer coefficient could be calculated.

Equipment

- 3 - "T" Type thermocouples
- 3 - Omega Ice Points
- 3 - Thermocouple Amplifiers with Low-Pass Filters (Measurements Group model 2310)
- 2 - Pitot Static Probes
- 2 - Differential Pressure Transducers
- 1 - Water Manometer
- 1 - 114 Ohm Thin Film Electrical Heater (Minco)
- 1 - Power Supply (Sorensen DCR-13B)
- 2 - Digital Multimeters (HP 34401A)
- 1 - AeroLab Tech Low Speed Wind Tunnel
- 1 - LabView Computer Board & Associated Software

Set-Up

1. The component was mounted in the center of the wind tunnel test section in a parallel orientation.
2. Airspeed Measurement - Pitot static probes were placed upstream and below the component. The total and static lines were routed in parallel to water manometer and differential pressure transducers. The differential transducers and wind tunnel airspeed recording instruments were zeroed. The manometer reading was sufficient for the larger airspeeds. However, at the low end of the airspeeds, the manometer accuracy was reduced and greater resolution was obtained from the tunnel and transducer readings. Nevertheless, the average of these four readings was used.
3. Temperature Measurement - Extra care was placed in mounting the thermocouples. For measuring surface temperature, a small dimple was placed in the center of the copper. The thermocouple end was placed inside the dimple and a punch was used to form the copper around the junction creating a mechanical joint. The wires were then carefully covered with electrical tape so that they did not act as pin fins. All wires were routed directly back in effort to keep the airflow undisturbed in front of the thermocouples. All thermocouples were zeroed to an Omega Thermocouple Calibrating Instrument.

Procedure

1. All instruments were turned on and were allowed to warm up for at least 30 minutes before being zeroed. Ambient conditions were recorded:

RUN1: 21 April 95 , 0600hrs

T ambient = 22.7 deg C

Pressure = 28.670 in Hg

%Rel Hum = 57%

RUN2: 28 April 95, 1700hrs

T ambient = 23.7 deg C

Pressure = 28.956 in Hg

%Rel Hum= 37%

RUN3: 12 Oct 95, 0800hrs

T ambient = 25.0 deg C

Pressure = 29.310 in Hg

%Rel Hum = 43%

2. Power supply was turned on and the component was allowed to stabilize in a natural convection environment (approx. 20 minutes)

3. Wind tunnel velocities were increased to 26.8 m/s and held until no temperature changes were observed on the component for a 200 second interval. The velocity and surface temperature readings were recorded. Data was recorded at freestream airspeeds 26.8, 22.4, 17.9, 13.4, 8.9, 4.5, and approx. 2-3 m/s

Computer Program

```
% This program takes surface temperature and freestream airspeed data and
% calculates h & Nu and compares the results against theoretical flat plate
% laminar flow correlations

% Air Properties from Incropera & Dewitt - Dry air 1-ATM
propty(:,1)=[250,300,350,400]';
propty(:,2)=10^(-6)*[11.44,15.89,20.92,26.41]';
propty(:,3)=[.72,.707,.700,.69]';
propty(:,4)=10^(-3)*[22.3,26.3,30,33.8]';

% Input Data (Temp-Kelvin, Velocity-MPH) and Calculate hx
Ts1=[339.15 320.65 312.15 308.35 306.15 304.25 302.75];
Velo1=(.447)*[4.53 9.13 19.44 29.3 39.43 49.95 60.19];
Ts2=[339.95 323.05 313.55 309.85 307.55 306.15 305.15];
Velo2=(.447)*[4.9 9.11 19.24 29.25 39.58 50.1 59.98];
power=19.55*.1735;
area=.0016;
flux=power/area;
Tamb1=22.75+273.15;
Tamb2=23.75+273.15;
for i=1:length(Ts1);
    hx1(i)=(flux/(Ts1(i)-Tamb1));
    hx2(i)=(flux/(Ts2(i)-Tamb2));
end

%Calculate hx from theory - Flat plate parallel, laminar flow
for j=1:length(Ts1);
    Tfilm1(j)=((Ts1(j)+Tamb1)/2);
    prop1=table1(propty,Tfilm1(j));
    hxtl(j)=.332*((Velo1(j)*.0222/prop1(1))^5)*(prop1(2)^(1/3))*prop1(3)/.0222;
    hxtt(j)=.0296*((Velo1(j)*.0222/prop1(1))^(4/5))*(prop1(2)^(1/3))*prop1(3)/.0222;
end

%Plot Heat Transfer Coefficient vs Velocity
plot(Velo1,hx1,'-',Velo2,hx2,'-',Velo1,hxtl,'-',Velo1,hxtt,'-',...
Velo1,hx1,'*',Velo2,hx2,'+',Velo1,hxtl,'x',Velo1,hxtt,'o'),...
title('Local Heat Transfer Coefficient vs Velocity'),...
ylabel('Local Heat Transfer Coefficient (watt/meter^2*K)'),...
xlabel('Velocity (meter/sec)')
pause
```

```

%Calculate log of Nussult & Reynolds Numbers
for j=1:length(Ts1);
    Tfilm1(j)=((Ts1(j)+Tamb1)/2);
    Tfilm2(j)=((Ts2(j)+Tamb2)/2);
    prop1=table1(prop1,Tfilm1(j));
    prop2=table1(prop2,Tfilm2(j));
    logRe1(j)=log10(Velo1(j)*.0222/prop1(1));
    logRe2(j)=log10(Velo2(j)*.0222/prop2(1));
    logNu1(j)=log10(hx1(j)*.0222/prop1(3));
    logNu2(j)=log10(hx2(j)*.0222/prop2(3));
    logNut1(j)=log10(.332*((Velo1(j)*.0222/prop1(1))^5));
    logNut2(j)=log10(.0296*((Velo1(j)*.0222/prop1(1))^(4/5)));
end

%Calculate Coefficients C, m C*Re^m
const(:,1)=[1,2]';
curve1=(polyfit(logRe1,logNu1,1))';
curve1(2)=10^curve1(2);
const(:,2)=curve1;
curve2=(polyfit(logRe2,logNu2,1))';
curve2(2)=10^curve2(2);
const(:,3)=curve2;
curve3=(polyfit(logRe1,logNut1,1))';
curve3(2)=10^curve3(2);
const(:,4)=curve3;
curve4=(polyfit(logRe1,logNut2,1))';
curve4(2)=10^curve4(2);
const(:,5)=curve4;
const

%Plot Dimensionless Representation of Heat Coefficient
%plot(logRe1,logNu1,'x',logRe2,logNu2,'o',logRe1,logNut1,'-',logRe1,logNut2,'-',...
%logRe1,logNu1,'*',logRe2,logNu2,'+',logRe1,logNut1,'x',logRe1,logNut2,'o'),...
for bg=1:length(Ts1);
    ln1(bg)=log10(curve1(2))+(logRe1(bg)*curve1(1));
    ln1(bg)=(ln1(bg));
    ln2(bg)=log10(curve2(2))+(logRe2(bg)*curve2(1));
    ln2(bg)=(ln2(bg));
end;
plot(logRe1,logNu1,'*',logRe2,logNu2,'+',logRe1,ln1,'-',logRe2,ln2,'-'),...
title('Dimensionless Representation of Heat Transfer Coefficient'),...
ylabel('Log Nussult/Prandtl'),...
xlabel('Log Reynolds Number')

```

Vita

Captain Thomas R. Layne was born on 5 March 1967, in Mt. Clemens, Michigan. He graduated from L'anse Creuse High School in 1985 and attended Michigan Technological University on an Air Force Scholarship. In 1989 he graduated Magna Cum Laude from Michigan Technological University, with a Bachelor of Science in Mechanical Engineering. After graduation he worked as an engineer at General Motors until being called into active duty in 1990. His first assignment was to the Atlas Launch Vehicles System Program Office, Space Systems Division, Los Angeles AFB, CA. In 1994 he was awarded the Air Force Association, General Samuel C. Phillips Award for Outstanding Young Engineer of the Year. In May 1994, he entered the Graduate School of Engineering, Air Force Institute of Technology.

Permanent Address: 38217 Mallast
Mt. Clemens, MI 48045

REPORT DOCUMENTATION PAGE			Form Approved OMB No. 0704-0188	
Public reporting burden for this collection of information is estimated to average 1 hour per response, including the time for reviewing instructions, searching existing data sources, gathering and maintaining the data needed, and completing and reviewing the collection of information. Send comments regarding this burden estimate or any other aspect of this collection of information, including suggestions for reducing this burden, to Washington Headquarters Services, Directorate for Information Operations and Reports, 1215 Jefferson Davis Highway, Suite 1204, Arlington, VA 22202-4302, and to the Office of Management and Budget, Paperwork Reduction Project (0704-0188), Washington, DC 20503.				
1. AGENCY USE ONLY (Leave blank)		2. REPORT DATE December 1995		3. REPORT TYPE AND DATES COVERED Master's Thesis
4. TITLE AND SUBTITLE VEHICLE THERMAL CONTROL WITH A VARIABLE AREA INLET			5. FUNDING NUMBERS	
6. AUTHOR(S) Thomas R. Layne				
7. PERFORMING ORGANIZATION NAME(S) AND ADDRESS(ES) Air Force Institute of Technology WPAFB, OH 45433-6583			8. PERFORMING ORGANIZATION REPORT NUMBER AFIT/GAE/ENY/95D-15	
9. SPONSORING / MONITORING AGENCY NAME(S) AND ADDRESS(ES) Dr. Richard Rivir WL/POTT 1950 Fifth St. Wright-Patterson AFB OH 45433-6523			10. SPONSORING / MONITORING AGENCY REPORT NUMBER	
11. SUPPLEMENTARY NOTES				
12a. DISTRIBUTION / AVAILABILITY STATEMENT Approved for public release; distribution unlimited			12b. DISTRIBUTION CODE	
13. ABSTRACT (Maximum 200 words) This study developed a variable area inlet and controller that regulated the temperature of an electrical component with ram air. The intent of the variable area inlet was to reduce vehicle drag by eliminating inefficiencies associated with component cooling and fixed area inlets. These inefficiencies arise from vehicles moving at varying speeds through varying air temperatures. The hardware model consisted of an electrical component mounted inside a right-circular cylindrical duct. The variable area inlet, mounted in the front of the duct, consisted of a butterfly valve that was actuated by a stepper controller acted on the feedback signal of a thermocouple that was mounted on the electrical component. The system was successful in regulating the component temperature. A nonlinear simulation model was built and the thermal plant in the simulation was based on the electrical component's empirically derived Nusselt number. Proportional, Proportional-Derivative (PD), and Proportional-Integral-Derivative (PID) controllers were built and tested. The PD and PID controllers did not appear to need any gain scheduling for the varying speed and temperature conditions. Lastly, a general design process was detailed.				
14. SUBJECT TERMS Thermal Control, Vehicle Drag, Internal Cooling Airflow, Variable Area Inlet			15. NUMBER OF PAGES 108	
			16. PRICE CODE	
17. SECURITY CLASSIFICATION OF REPORT Unclassified	18. SECURITY CLASSIFICATION OF THIS PAGE Unclassified	19. SECURITY CLASSIFICATION OF ABSTRACT Unclassified	20. LIMITATION OF ABSTRACT UL	